



# The metasedimentary-hosted Nyangoubé gold prospect, northwest Côte d'Ivoire: Geochemical and mineralogical characterization of associated hydrothermal alteration

Lipoublida Djagre<sup>a,\*</sup>, Barthélémy Gnammytchet Koffi<sup>a</sup>, Moussa Camara<sup>a</sup>, Gbele Ouattara<sup>a</sup>, Yao Agbossoumonde<sup>b</sup>

<sup>a</sup> Department of Earth Sciences and Mining Resources (STeRMi), Civil Engineering Laboratory, Geosciences and Geographical Sciences, Institut National Polytechnique Félix Houphouët-Boigny, Yamoussoukro, Côte d'Ivoire

<sup>b</sup> Department of Geology, Faculty of Sciences, University of Lomé, Togo

## ARTICLE INFO

### Keywords:

Nyangoubé  
Hydrothermal alteration  
Geochemistry  
Prospect  
Mineralization  
Gold

## ABSTRACT

The Nyangoubé gold prospect, located in northwestern northwest of Côte d'Ivoire in Africa, is a feature of the Bagoé furrow of the Birimian of the West African Craton. This study is aimed at characterizing the geochemical and mineralogical signatures of hydrothermal alterations associated with the gold mineralization of Nyangoubé gold prospect to provide guidelines for mining exploration. Microscopic petrographic analysis and geochemical characteristics from elemental contents analyzed by X-ray fluorescence (XRF) and inductive coupled-plasma mass spectrometer (ICP-MS) were studied using alteration diagrams and by calculating mass balances and describing thin sections. The results indicate that the host rocks have been affected by silicification, carbonation, sericitization, chloritization, sulphidation and albitization. Hydrothermal alterations associated with the mineralization systems resulted in the destruction of plagioclase in the metasediments studied. The latter was replaced by sericite, chlorite, carbonates, quartz, and sulphides in varying proportions, depending on the intensity of each type of alteration linked to the formation of each mineral. The mass balance calculations show a gradual increase in the concentrations of Au, W, V, As and Pb as well as K<sub>2</sub>O, CaO, Na<sub>2</sub>O and Fe<sub>2</sub>O<sub>3</sub> which could be vectoring parameters towards gold mineralization. The mineralogical assemblage as sericite-chlorite-pyrite, chlorite-pyrite±sericite, carbonate-sericite and chlorite-carbonate revealed by hydrothermal alteration trends in the host rocks could also help identify potential gold corridors in the area of study and its peripheries.

## 1. Introduction

Most gold occurrences in the Paleoproterozoic grounds of the West African Craton are orogenic gold deposits formed during the Eburnian cycle about two billion years ago [1–4]. The formation of these deposits is directly related to crustal accretion or collisional processes in a subduction context and can be developed in arc, back-arc or accretionary prism environments [5]. The significant magmatic activity allows their formation and the circulation of hydrothermal fluids from the devolatilization of the

\* Corresponding author.

E-mail address: [lipoublida.dja@gmail.com](mailto:lipoublida.dja@gmail.com) (L. Djagre).

<https://doi.org/10.1016/j.heliyon.2023.e20227>

Received 16 March 2023; Received in revised form 13 September 2023; Accepted 14 September 2023

Available online 16 September 2023

2405-8440/© 2023 The Authors. Published by Elsevier Ltd. This is an open access article under the CC BY-NC-ND license (<http://creativecommons.org/licenses/by-nc-nd/4.0/>).

volcano-sedimentary pile during prograde metamorphism, most commonly greenschist metamorphic facies [6,7]. These deposits are hosted in different lithologies characterized by mineralogical assemblages assigned to one or more hydrothermal alteration episodes. Hydrothermal alteration in these host lithologies is characterized by signatures that vary chemically, mineralogically and spatially from proximal to distal depending on the deposit type [8,9]. The circulation of fluids through the host rocks causes mineralogical changes that are manifested by transformations in the mineralogical assemblage present [10]. Thus, hydrothermal alteration is directly associated with the genesis of some types of gold and metal deposits, and are a discriminating feature that influences mineral resource exploration techniques.

The Nyangoubé gold prospect, located in northwestern Côte d'Ivoire, is part of the Birimian unit of the West African craton. The study of associated hydrothermal alteration is a means of determining the various hydrothermal vectors related to the mineralization of this prospect. In addition, gold occurrences in Côte d'Ivoire are hosted in different petrographic units metamorphosed to greenschist facies and hydrothermally altered. This is the case of the Bonikro gold deposit, in central Côte d'Ivoire, where gold mineralization is hosted in metasediments and granodiorites [11]. To the southeast, in the Afema deposit, gold occurrences are hosted mainly in metasedimentary formations [12]. In the Agbahou, Hiré and Dougbafla-Bandama deposits, gold mineralization is found in a complex system of subparallel or oblique quartz veins hosted in mafic volcanic and volcano-sedimentary rocks [13,14].

In this study, we characterized the geochemical and mineralogical signatures of hydrothermal alterations associated with the gold mineralization of prospects by documenting their geochemistry, paragenesis and petrography. This will make it possible to determine the hydrothermal footprint of the gold system and propose hydrothermal vectors towards the mineralized sectors with the aim of proposing guides for exploration. On this basis, we illustrated the mobility of chemical elements during hydrothermal alteration; extracted parameters to map the intensity and distribution of fluid and rock interacts from alteration diagrams, and provided mass balance calculations and petrographic descriptions.

## 2. Geological context

Located in the southern part of the West African craton, precisely in the Man Ridge, the geological formations of Côte d'Ivoire are divided between two chronologically distinct units. The coastal sedimentary basin of secondary-tertiary age occupies 2.5% of the

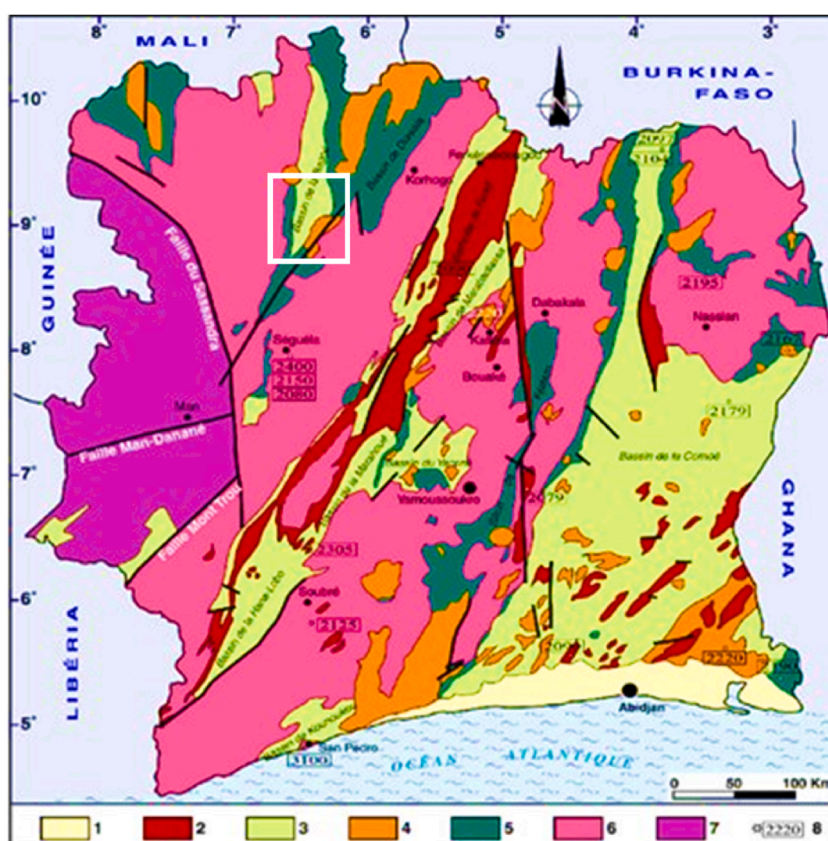


**Fig. 1.** Simplified map of the geological units of the Ivory Coast [17]. 1: Ferké batholith, 2: two-mica granitoids associated with meridional dipping structures; 3: other two-mica granites; 4: sedimentary basins and volcano-sedimentary units; 5: Calc-alkaline granitoid localized in sedimentary basins; 6: Calc-alkaline granitoid localized in greenstone belts; 7: Undifferentiated granitoid, banded granites, gneisses, and migmatites (age above 2.4 Ma); 8: Periods.

territory (Fig. 1) and the Precambrian basement occupies 75.5% of the country [15]. The Precambrian basement consists of formations that are distributed in two domains of the Man Ridge. These are the Kénéma-Man domain of the Archean age and the Baoulé-Mossi domain of the Lower Proterozoic age, which are separated by the Sassandra fault [16].

### 2.1. Archean domain

The Archean domain is located in the west of the Sassandra Fault and it is structured by two orogenies: the Leonian (3.5–2.9 Ga) and the Liberian (2.9–2.5 Ga). The Liberian orogeny is the most pronounced magmatic and metamorphic event in the Archean domain of the Man Ridge [18]. From a lithological point of view, two major groups are distinguished by Wood in Ref. [19] a basic complex made up essentially of migmatites and granulitic gneisses, normally referred to as grano-gneiss; the second group constitutes the belts of supracrustal rocks that lie unconformably on the first group. Granites and charnockites are associated with these two groups in the form of intrusions in the granite-gneissic basement. Legoux [20] defined the basic complex of the Archean domain of Côte d'Ivoire for the first time, describing it as a continuous complex that extends from a granitic pole to a northerly pole and includes all leucocratic orthoclase or microcline rocks expressed in the granitic series. Within this granitic series, he defined calc-alkaline granites, aplogranites, perthite granites and hypersthene granites. In the northern series, he also described leucocratic to melanocratic rocks characterized by the presence of plagioclase and magnesian pyroxene [20]. For some authors, the lithology of the Archean domain of Côte d'Ivoire consists mainly of formations from the Liberian cycle and includes green rocks (metabasalt, metarhyolites, metadacite, metarhyodacite ...), which metamorphic gradient varies from the facies of amphibolites to the granulites facies with, migmatites, leptynites, charnockites, banded quartzites and trondhjemitites [21,22]. These formations are intruded by basic to ultrabasic complexes and granite-gneissic complexes.

### 2.2. Baoulé-Mossi domain

Located in the east of the Sassandra Fault, the Baoulé-Mossi domain of Côte d'Ivoire is structured by the Eburnian (2.15–1.18 Ga) and Burkinian (2.5–2.15 Ga) orogenies [22]. This domain is made up of seventeen furrows or volcano-sedimentary basins distributed over two alignment trends such as Tehini-Dimbokro, in the east, and Ferkessédougou-Soubéré in the center [22,23]. The lithological formations of this domain are thus characterized by volcano-sedimentary, volcanic, and meta-sedimentary complexes that alternate along the NNE-SSW Birimian direction. Within these rocks granitoid batholiths are intruded; these are composed of granites, granodiorites, and tonalities. Greenstone belts composed of metabasalts, metagabbros, metarhyolites, metarhyodacites, metadacites and amphibolites are found in these formations [22,24,25]. In central Côte d'Ivoire, the mafic rocks of the Toumodi-Fétékro belt are less evolved with a greater dominance of gabbro accumulation. This belt is dominated by granitic plutons dated at  $2144 \pm 6$  Ma [25, 26]. Volcanic and calc-alkaline formations are abundant and have evolved from andesites to rhyolites [27] with the rhyolites dated at  $1505 \pm 1$  Ma. The sedimentary formations were metamorphosed in contact with the granites emplaced and dated at  $2084 \pm 6$  Ma and  $2079 \pm 11$  Ma [28]. The mafic formations of Toumodi are metamorphosed by two granites dated to  $2151 \pm 3$  Ma [29]. A metarhyolite rock believed to belong to the belt gives a zircon age of  $2195 \pm 6$  Ma [30]. In the upper Comoé belt, andesitic volcanic rocks are interstratified in the clastic sedimentary strata that were deposited above the first-generation granitoid [26,31]. In the northwest of

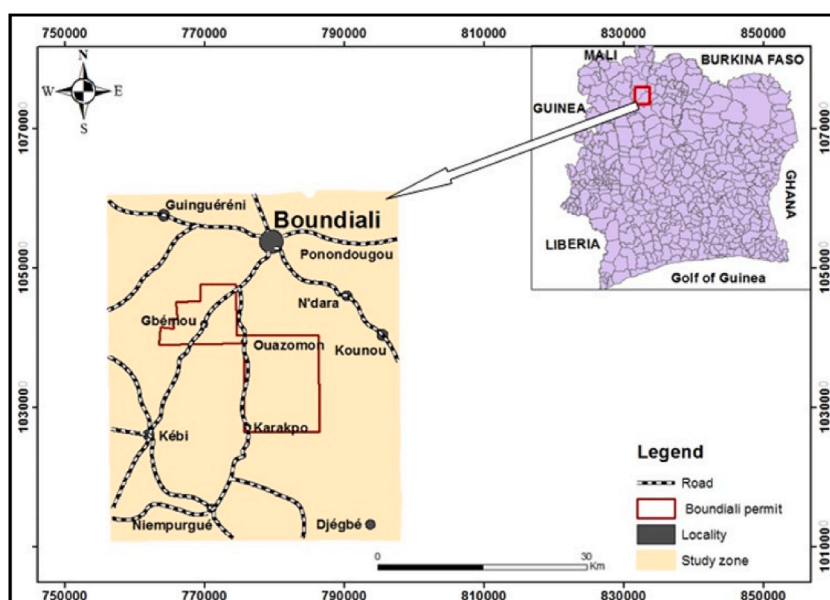


Fig. 2. Location of the study area.

Côte d'Ivoire, the green rocks are tholeiitic and covered by clastic sediments from the Bagoé basin which include lava intercalated with andesites and rhyolites [32,33]. To the north of the Bagoé basin, in southern Mali, a rhyodacite associated with sediments is dated at  $2098 \pm 5$  Ma, while a granodiorite which intruded into the basin is dated at  $2074 \pm 9$  Ma [34].

Structurally, the Eburnian cycle of the Baoulé-Mossi domain is thought to be affected by three phases of tectonic deformation [35–37]: i) the first phase of tangential deformation ( $D_1$ ) is thought to be responsible for the creation of the Eburnian trenches; ii) the second phase ( $D_2$ ) is thought to be responsible for the second generation of Eburnian folds. This deformation is accompanied by a sub-vertical schistosity  $S_2$  that folds the  $S_1$  schistosity; iii) the third phase of deformation ( $D_3$ ), also transcurrent in nature, was probably responsible for the setting of the  $P_3$  folds and associated with the foliation and would be at the base of the creation of the “canals” of crushing.

The Boundiali furrow, to which our study area belongs, is an entity of the Baoulé-Mossi domain, known as Boundiali-Bagoé, located in the northwest of Côte d'Ivoire in the department of Boundiali (Fig. 2). The geological formations in this trench are of the Paleoproterozoic age and arranged in the form of a syncline [38]. They are characterized by a succession of bands of migmatic, plutonic and schistose rocks surrounded by granites belonging to the Madinani wrinkle and the southern part of the Niélé wrinkle, which Haut-Marahoué formations' constitute the base of the syncline synclinal [39]. These formations are thus dominated by undifferentiated schists, muscovite mica-schists, biotite, epidote, amphibole schists, quartzites and amphibole schists (Fig. 3).

### 3. Materials and methods

Due to the absence of outcrops caused by the effects of weathering, the methodological approach used in this study was applied exclusively to samples taken from exploration drill cores of the geological formations hosting the mineralization of the gold prospect of Nyangoubé.

The petrographic examination was carried out on a set of 24 thin slides prepared and observed under optical microscopy at the Bedrock Geology and Metallogeny Laboratory (UFR-STRM). The geochemical data acquired are from two sources. The first source comes from the analyses that we have carried out in the framework of this work. The second is unpublished data from the mining company, Turaco Gold, which holds the exploration permit of the study area. For the first source data, 20 exploratory drill core samples were analyzed. Whole-rock geochemical analyses were performed at Bureau Veritas Commodities Canada Ltd laboratory in Vancouver, Canada. Fifty-eight chemical elements were assayed according to the LF600 package (XF700-LF100-AQ200). The analysis of each element is independent of its specificity and the type of chemical analysis. Major elements were analyzed by X-ray fluorescence (XRF) except for  $Cr_2O_3$  which was analyzed by inductively coupled plasma mass spectrometry (ICP-MS). The detection limit of these

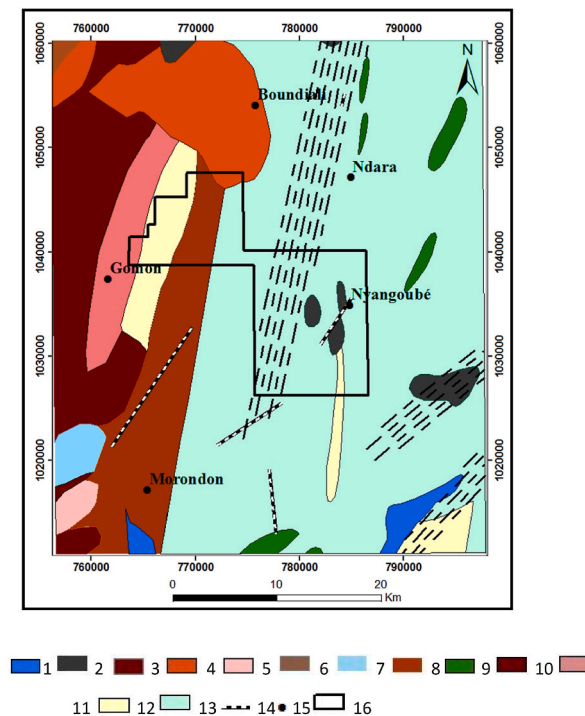


**Fig. 3.** Geological map of the study area extracted from the Boundiali geological sheet at 1:200 000 [40]. 1. Andesitic breccia 2. Gabbro 3. Biotite granite 4. Granite with biotite and porphyritic facies 5. Biotite-hornblend granodiorite 6. Biotite migmatite 7. Mozonite mozogranite 8. Metaarenite 9. Metagabbro, amphibolite 10. Biotite metagranite 11. Biotite metagranodiorite 12. Quartzites 13. Undifferentiated shale 14. Faults 15. City 16. Boundiali permit.

elements analyzed by the XF700 method is 0.01%. The loss on ignition (LOI) is obtained after heating the samples to 1000 °C. Base metals such as Ag, Co, Cu, Mo, Ni, Pb, Zn and Cd are obtained by the AQ200 analytical method followed by their determination by atomic emission spectrometry (ICP-AES). Trace elements and rare earth elements were obtained by lithium metaborate fusion and analyzed by inductively coupled plasma mass spectrometry (ICP-MS). Volatile elements and gold were analyzed by Aqua Regia digestion (AQ200) and quantified by ICP-MS. The representative set of geochemical analyses for these samples is recorded in [Tables 1 and 2](#).

Data from the second source consists of 126 samples from destructive Aire Core (RC) drilling. These samples were subjected to two types of analytical methods: ICP-MS analysis and XRF analysis.

For the XRF analysis, the samples were analyzed by Turcot Gold using the portable XRF machine to determine the major elements and base metals. In the case of ICP-MS analysis, these samples were sent to the Veritas Commodities Canada Ltd laboratory in Vancouver, Canada. The samples also went through the same analytical processes as the others (first source samples). This method of analysis made it possible to obtain from these samples the contents of trace and rare earth elements, volatile elements, and gold. The complete set of analyses of these samples is available from corresponding author. The geochemical data were used to construct binary and ternary diagrams to discriminate the intensity of hydrothermal alteration and to calculate mass balance to quantify the mobility of chemical elements during hydrothermal alteration. For mass balance calculations, it is obvious to have the immobile referential elements of the altered rocks and those of their precursors, because the pairs of immobile elements keep constant ratios during the alteration. For this purpose, the single precursor method of Gresens [41] was used to evaluate chemical changes of hydrothermally altered country rocks.

## 4. Results

The metasedimentary units constitute the wall rocks of the gold mineralizations of the Nyangoubé prospect. These units are affected by penetrating schistosity and fracture schistosity expressed by chlorite, sericite, and fracture planes. They are commonly oriented N–S to NNE–SSW, dipping subvertically. These formations are difficult to determine on the surface due to the effects of saprolitization and lateritization phenomena that can reach depths of up to 70 m. They have been deformed regionally in a cataclastic and partly ductile way, producing an undulation of certain minerals such as quartz.

### 4.1. Geochemistry of alterations

#### 4.1.1. Classification of rocks

The geochemical classification of metasedimentary rocks is based on the method of Fralick [42] using the  $Al_2O_3/TiO_2$  binary diagram. The purpose of this diagram is to identify groups of  $Al_2O_3/TiO_2$  pairs that can highlight potential sedimentary sources represented by straight lines through the origin ([Fig. 4A](#)). The diagram distinguishes four groups of sedimentary rocks called groups 1, 2, 3 and 4 with  $TiO_2$  contents of between 0,52% and 0,69%, 0,69% - 0,74%, 0,47–0,79% and 0,79–1,56%. Each group consisted of 57, 27, 32 and 30 metasedimentary rock samples respectively.

**Table 1**  
Geological data of the different analyzed samples.

Elements	B1	B2	B2	B4	B5	B6	B7	B8	B9	B10
SiO <sub>2</sub> (%)	68.70	51.26	65.02	65.30	66.15	4.4	73.46	69.47	56.82	56.31
TiO <sub>2</sub>	0.57	1.00	0.68	0.64	0.75	0.12	0.48	0.62	0.72	0.67
Al <sub>2</sub> O <sub>3</sub>	15.22	24.30	16.49	15.32	12.73	62.38	12.62	14.33	19.69	19.64
Fe <sub>2</sub> O <sub>3</sub>	5.68	7.93	7.37	6.65	7.92	14.25	3.05	5.71	8.38	8.47
MnO	0.08	0.08	0.05	0.10	0.13	2.12	0.06	0.06	0.06	0.05
MgO	1.60	2.25	1.80	2.28	2.60	3.78	0.81	1.51	3.29	3.56
CaO	2.21	1.72	1.18	3.92	4.15	7.88	1.68	2.45	1.40	1.18
Na <sub>2</sub> O	2.87	2.67	1.87	2.23	3.46	3.92	3.42	3.11	2.34	2.27
K <sub>2</sub> O	2.56	5.45	2.30	0.39	1.30	3.62	3.77	2.07	3.12	3.02
P <sub>2</sub> O <sub>5</sub>	0.12	0.20	0.15	0.12	0.20	0.74	0.16	0.12	0.10	0.12
LOI (%)	0.96	3.07	2.57	2.18	1.17	0.05	0.39	1.18	3.42	3.70
Total	<b>100,57</b>	<b>99,93</b>	<b>99,48</b>	<b>99,13</b>	<b>100,56</b>	<b>103,26</b>	<b>99,9</b>	<b>100,63</b>	<b>99,34</b>	<b>98,99</b>
Rb(ppm)	80.6	151.6	82.0	13.4	61.9	8.2	161.2	66.4	107.4	101.7
Sr	266.2	281.7	215.4	265.2	511.2	1	275.2	347.1	242.3	240.3
Ba	564	1578	437	216	319	<0.02	750	665	657	531
Zr	133.7	211.3	163.2	143.4	144.9	1.4	261.8	181.9	138.3	124.6
Pb	2.4	4.0	3.0	2.7	1.8	31.5	5.8	3.2	4.4	3.7
Th	5.3	8.6	5.8	4.7	5.8	0.6	7.1	6.7	6.7	6.2
Cs	3.0	5.0	4.5	1.1	2.6	27.4	6.6	2.2	4.1	3.3
V	93	184	124	112	129	2.3	30	96	159	146
W	3.0	6.6	9.9	10.3	1.0	149	<0.5	3.0	12.7	13.8
As	43.8	112.6	0.8	1.1	1.2	37.1	<0.5	390.6	22.1	85.7
Eu	1.05	1.57	1.13	1.00	1.21	6.60	1.24	1.16	1.30	1.23
Ta	0.4	0.9	0.5	0.5	0.4	452.4	1.5	0.5	0.6	0.5
Au(ppb)	4.1	16.4	154.0	8.0	28.7	<0.1	1.3	17.9	24.2	6.8

**Table 2**  
Geological data of the different analyzed samples.

Elements	B11	B12	B13	B14	B15	B16	B17	B18	B19	B20
SiO <sub>2</sub> (%)	62.06	99.60	70.22	66.82	67.07	1.9	50.55	45.74	78.16	51.07
TiO <sub>2</sub>	0.78	0.04	0.53	0.69	0.76	0.06	1.18	1.12	0.06	1.56
Al <sub>2</sub> O <sub>3</sub>	18.47	0.24	13.76	14.35	16.29	70.90	14.19	14.11	11.61	13.63
Fe <sub>2</sub> O <sub>3</sub>	6.98	0.64	4.31	6.54	6.99	13.09	12.99	13.86	0.97	15.18
MnO	0.05	0.02	0.06	0.09	0.05	1.74	0.14	0.17	0.02	0.11
MgO	1.91	<0.01	1.56	2.59	1.86	1.27	3.93	4.45	0.06	3.86
CaO	0.45	0.01	3.27	3.46	0.55	6.26	4.80	7.13	0.74	4.39
Na <sub>2</sub> O	1.36	<0.01	3.84	3.09	1.49	2.35	4.40	3.54	2.66	3.37
K <sub>2</sub> O	3.81	0.04	0.99	1.52	2.07	1.49	0.32	0.43	5.36	0.35
P <sub>2</sub> O <sub>5</sub>	0.13	<0.01	0.10	0.19	0.14	0.50	0.10	0.09	0.03	0.11
LOI (%)	3.02	0.34	1.25	1.41	2.72	0.04	7.38	9.53	0.36	4.98
<b>Total</b>	<b>99,02</b>	<b>100,96</b>	<b>99,89</b>	<b>100,75</b>	<b>99,99</b>	<b>99,6</b>	<b>99,98</b>	<b>100,17</b>	<b>100,03</b>	<b>98,61</b>
Rb(ppm)	7.2	0.2	5.7	6.4	7.0	2.7	3.9	2.7	1.8	4.6
Sr	110.3	10.2	276.8	304.7	171.1	<1	213.6	204.7	173.5	156.5
Ba	728	18	188	302	394	0.52	133	123	638	117
Zr	162.4	7.8	168.9	156.3	153.4	5.3	92.5	75.1	78.9	103.9
Pb	52.9	3.5	47.1	29.4	28.3	0.5	106.1	79.3	1.3	79.3
Th	5.8	<0.2	5.2	5.3	5.4	0.4	1.3	0.6	6.6	0.8
Cs	2.7	<0.1	3.2	2.3	2.2	15.5	0.4	0.7	3.2	0.7
V	154	18	84	117	123	1.4	278	278	<8	363
W	8.9	5.8	0.7	5.7	9.2	91	3.1	11.7	2.8	9.5
As	128.8	1.7	77.9	28.6	21.3	39.2	111.8	185.4	1.1	601.4
Eu	0.91	0.13	1.18	1.56	1.31	4.51	1.07	0.94	0.42	1.10
Ta	0.5	<0.1	0.4	0.4	0.5	172.3	0.3	0.2	0.2	0.4
Au(ppb)	20.5	2.0	3.9	9.5	3.3	<0.1	11.2	8.7	<0.5	15.2

To name the different groups distinguished, the binary graph of Herron [43] has been illustrated. In this diagram (Fig. 4B), the groups of metasedimentary rocks are mainly divided into shales (schists, argillites), pelites and conglomerates; as well as greywackes, sandstones, and arkosic arenites. Each group was also subdivided into subgroups according to their degree of hydraulic fractionation due to the erosion of the rocks which edify particles of different sizes. These particles are therefore classified differently during their deposition because large particles and fine particles do not have the same hydraulic properties [44]. Geochemical and compositional fractionation of particles is based on their hydraulic sorting. Chemical particles that are particularly concentrated in the clay fractions of pelites include: Al<sub>2</sub>O<sub>3</sub>, MgO, K<sub>2</sub>O, Fe<sub>2</sub>O<sub>3</sub>, TiO<sub>2</sub>, Zn, Cr, Sc, Rb, Y and Cs, as well as heavy rare earth elements (HREE) [44,45]. The particles of the sandy fractions of the greywackes, mainly composed of feldspars and quartz, are dominated by SiO<sub>2</sub>, Na<sub>2</sub>O, CaO, Th, Zr, Hf and light rare earth elements (LREE) [45]. To illustrate the phenomenon of hydraulic sorting, it will be necessary to couple a less mobile element (Al<sub>2</sub>O<sub>3</sub>) of the clay fraction to another of the sandy fraction (Zr) (Fig. 4C). A precursor is determined for any fractionation/source combination in order to limit primary composition variations. The graph illustrating the process of hydraulic sorting (Fig. 4C) shows that the rocks of group 1 underwent hydraulic splitting allowing them to be grouped into three precursors (subgroups). The rocks of groups 2, 3 and 4 do not show a clear tendency to hydraulic splitting. A single precursor has been attributed to these groups due to their small number.

#### 4.1.2. Behavior of major elements

Hydrothermal alteration affecting the metasedimentary rocks, hosting gold mineralization, has a strong impact on the various major elements of the latter. Harker diagrams contrasting SiO<sub>2</sub> with other major elements not only show SiO<sub>2</sub> variation about the latter but also the influence of alteration on the chemical composition of the metasedimentary rocks (Fig. 5). In these diagrams, aluminium (Al<sub>2</sub>O<sub>3</sub>), titanium (TiO<sub>2</sub>) and iron (Fe<sub>2</sub>O<sub>3</sub>) show very little variation except for a few samples. On the other hand, potassium (K<sub>2</sub>O), sodium (Na<sub>2</sub>O), magnesium (MgO) and calcium (CaO) show a much more erratic pattern with sample distribution. These correlations of major elements are important since they constitute components in the mineral phases that characterize potassium (sericitic), carbonate and chlorite alterations. To quantify hydrothermal alteration from major elements, it is necessary to define the alteration vectors with which they are associated from the ternary and binary diagram of alteration.

#### 4.1.3. Ternary diagrams

The diagram in Fig. 6A consists of three poles, each of which represents an alteration mineral. The FeO + MgO, Na<sub>2</sub>O + CaO, and K<sub>2</sub>O poles represent chlorite, plagioclases and, sericite respectively. In this diagram, the alteration vectors start from the plagioclase pole towards the poles associated with chlorite and sericite, or towards the opposite axis which represents biotite. The A-CNK-FM ternary diagram of Nesbitt et al. [46] (Fig. 6B) shows an alteration vector towards the chlorite and biotite poles. The samples of the metasedimentary groups then approach these poles. There was therefore a considerable contribution of K<sub>2</sub>O, MgO and FeO in the metasediments during hydrothermal alteration.

**4.1.3.1. Sericite and albite alteration indices.** The use of alteration indices allows the characterization of the type and intensity of alteration of the different metasedimentary groups to understand the chemical and mineralogical modifications during the circulation

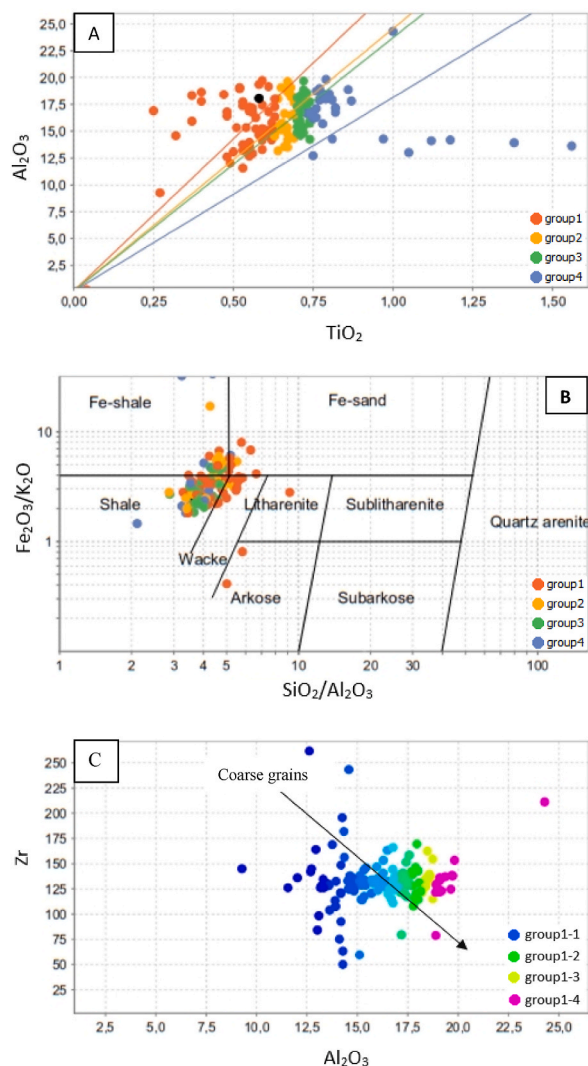


**Fig. 4.** Classification and nomenclature of metasediments: A) diagram defining the potential sources of metasediments, B) diagram of [43] applied to metasediments, C) diagram illustrating the hydraulic fractionation of metasediments.

of mineralizing fluids.

The sericite, albite and sericite-albite binary saturation diagrams established by Kishida et al. [47] (Fig. 7) are commonly used to characterize alkaline alteration associated with hydrothermal gold deposits. In these plots, sericite (Fig. 7 C), albite (Fig. 7 B) and sericite-albite (Fig. 7C) saturation indices increase proportionally in relation to alumina ( $\text{Al}_2\text{O}_3$ ) content. This suggests that these samples were affected by strong potassium and sodium alteration. Under these conditions, samples from the metasedimentary groups are enriched in  $\text{K}_2\text{O}$  and  $\text{Na}_2\text{O}$  and depleted in  $\text{MgO}$ .

**4.1.3.2. Box plot alteration diagrams.** Whisker boxes are graphical representations that use weathering indices (the Ishikawa weathering index (AI) and the chlorite-carbonate-pyrite weathering index (CCPI) to quantify weathering intensity (Fig. 8). In these diagrams, the metasedimentary rock groups show higher AI and CCPI values except for a few samples that show low values. This suggests a reduction in the mobility of alkali elements and  $\text{CaO}$  in the different metasedimentary rock groups. These rocks are constitutionally sub-alkaline and meta-aluminous. The alteration index AI ranges from 20 to 50 for samples of poorly altered metasedimentary groups and from 50 to 100 for samples of more hydrothermally altered metasedimentary rocks (Fig. 8A). This index is therefore designed to evaluate the main formation elements of these metasedimentary rocks during sericite and chlorite alteration ( $\text{K}_2\text{O}$ ,  $\text{MgO}$ ) over the elements gained and lost ( $\text{K}_2\text{O}$ ,  $\text{MgO}$ ,  $\text{CaO}$ ,  $\text{Na}_2\text{O}$ ).

The correlation between  $\text{Na}_2\text{O}$  and AI of the different metasedimentary rock groups is shown in Fig. 9A. This diagram describes the leaching of  $\text{Na}_2\text{O}$  as a function of increasing AI. In this graph, the rock samples show a trend from the albite to the chlorite-sericite domain with an increase in AI and a decrease in  $\text{Na}_2\text{O}$ . There is a strong correlation between AI and sodium ( $\text{Na}_2\text{O}$ ) depletion

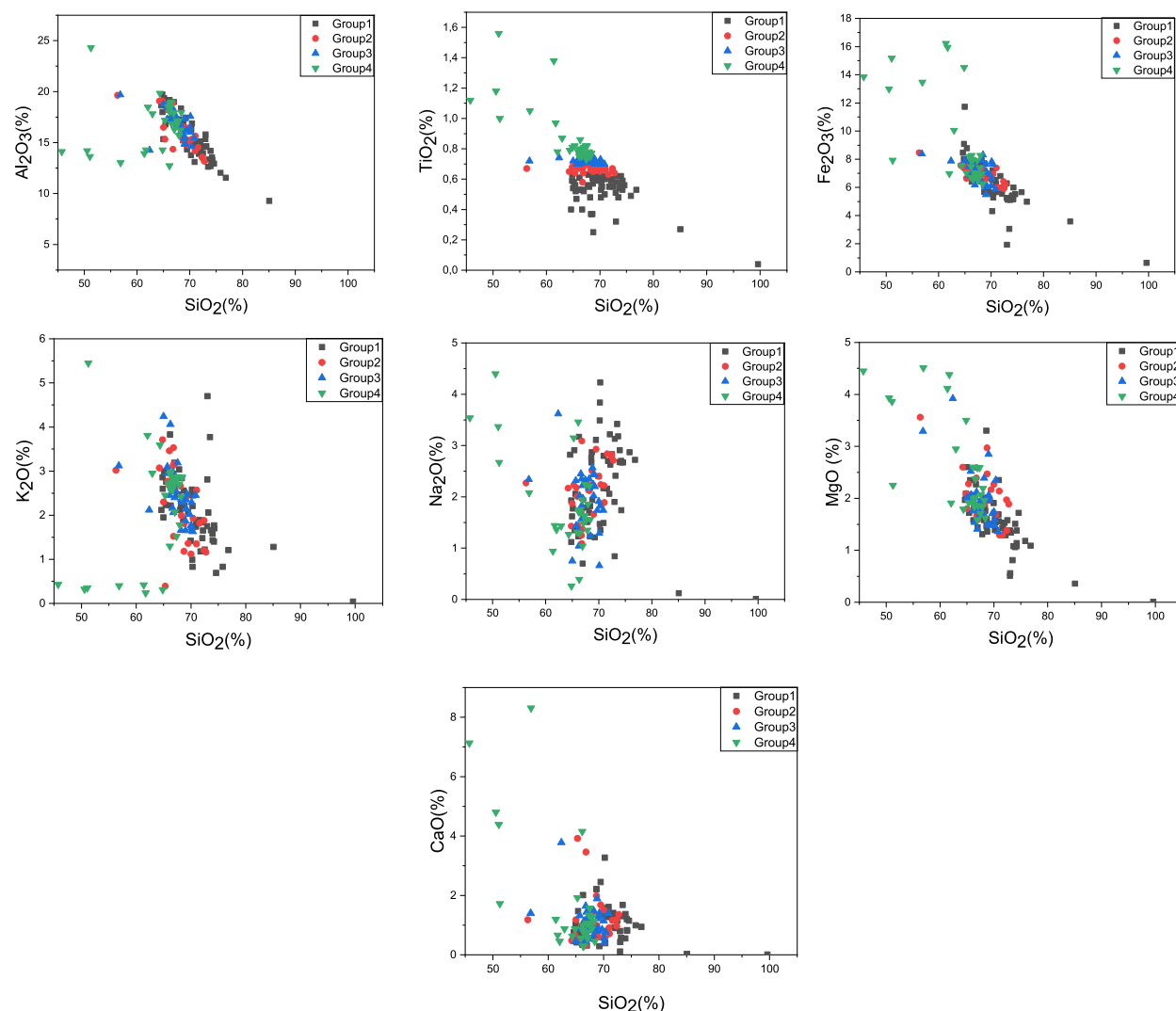


**Fig. 5.** Harker diagrams contrasting major oxides with  $\text{SiO}_2$  of different geochemical groups of metasedimentary rocks.

because sodium depletion is the main chemical exchange involved in the degradation of sodium plagioclase [48]. This index has proven to be very useful in mineral exploration by providing a quantitative estimate of the intensity of hydrothermal alteration related to gold mineralization, increasing to maximum values in the hydrothermal vent zone below the gold-bearing ore lenses [49].

In Fig. 9B, the increase in AI is accompanied by an increase in  $\text{K}_2\text{O}$  content.  $\text{K}_2\text{O}$  enrichment in these samples is dependent on the sericite/chlorite ratio ( $\text{K}_2\text{O}/\text{MgO}$ ) in the weathered products. The AI has two limitations: it does not take into account carbonate alteration, which can be significant in some alteration systems and can lead to its decrease even when alteration intensity increases. It also does not distinguish extensive chlorite alteration from sericite-rich alteration because both common alteration types are associated with massive sulfide ores [50].

The CCPI quantifies the increase in MgO and FeO associated with the development of chlorite that commonly replaces potassium feldspar and albite in a hydrothermal alteration system (Fig. 8 B). It is also positively dominated by carbonate alteration as well as pyrite, hematite, or magnetite enrichment.

The box plot in Fig. 10 is a binary graphical representation combining the IA plotted on the x-axis and the CCPI plotted on the y-axis. In this diagram, samples from the less altered metasedimentary rock groups fall in the center bounded by the AI index ranging from 25 to 70 and the CCPI index ranging from 40 to 80. Those that are more strongly altered are located at variable positions according to the main hydrothermal minerals (chlorite, sericite, pyrite, potassium feldspar, albite, ankerite, dolomite and epidote) present and located along the box plot boundaries. The progressive variation of alteration is appreciated by comparing different positions of the samples in the diagram. The least altered samples below the diagonal connecting the epidote pole and the potassium feldspar pole preserved primary albite with minor chlorite and sericite development that is appreciated as associated with greenschist facies metamorphism and not with hydrothermal alteration (Fig. 10). The least altered samples above the diagonal are characterized



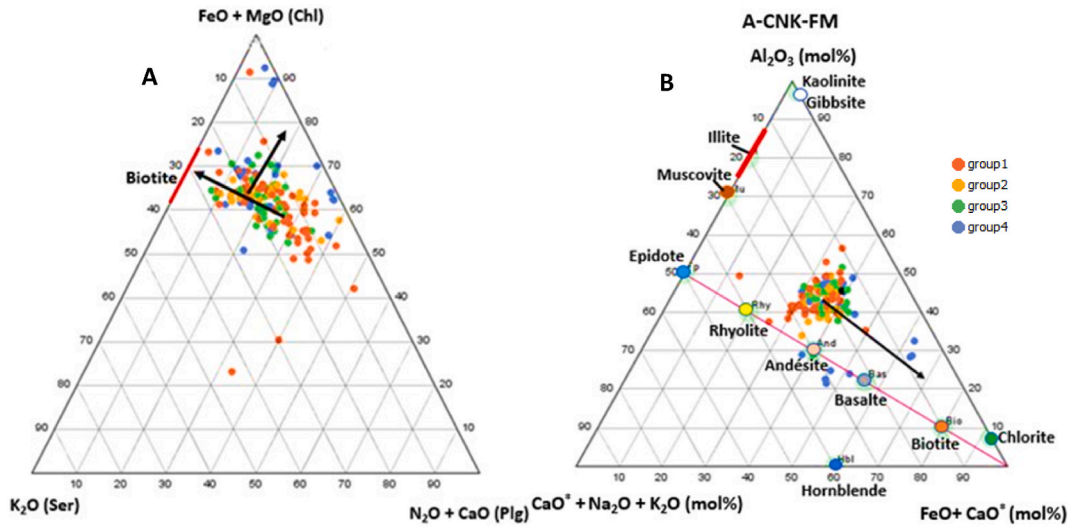


Fig. 6. Ternary diagrams with poles showing hydrothermal alteration minerals in metasedimentary rocks hosting the Boundiali gold prospect; A-CNK-FM ternary diagram of [46] (A), and FeO + MgO/K<sub>2</sub>O/Na<sub>2</sub>O + CaO diagram (B) shows the hydrothermal alteration vectors approaching the chlorite and biotite poles.

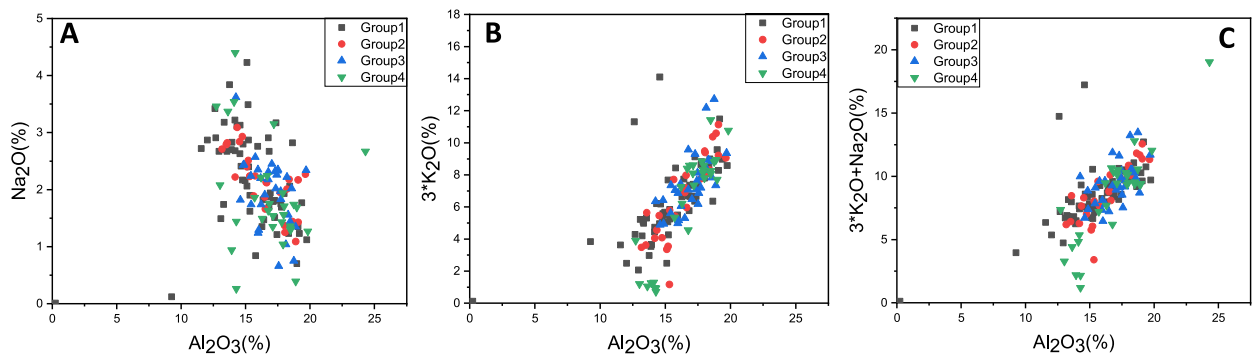


Fig. 7. Binary saturation diagrams, A) sericite ( $3^*K_2O/Al_2O_3$ ), B) albite ( $Na_2O/Al_2O_3$ ), C) sericite albite ( $3^*K_2O + Na_2O/Al_2O_3$ ), applied to the metasedimentary rocks hosting the Boundiali gold prospect.

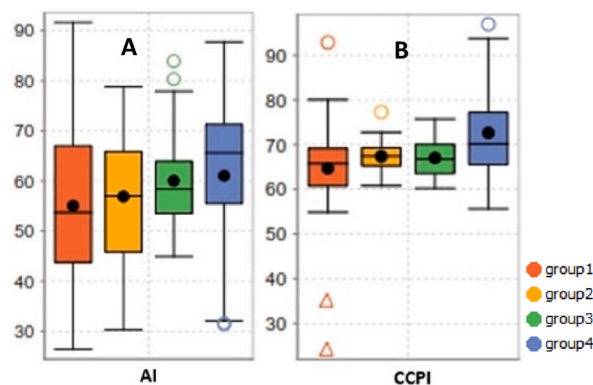


Fig. 8. Box plots showing the variation of alteration indices AI (A) and CCPI (B) in the metasedimentary rocks hosting the Boundiali gold prospect.

by a sericite-carbonate alteration trend (vector 5 trend). The most hydrothermally altered and following trends 3 and 4 alteration vectors are intensely altered to a sericite-chlorite-pyrite characteristic of the lower sponge alteration system of mineralization within the metasediments, and chlorite-pyrite ± sericite characteristic of the lower sponge alteration of mineralization dominated by chlorite

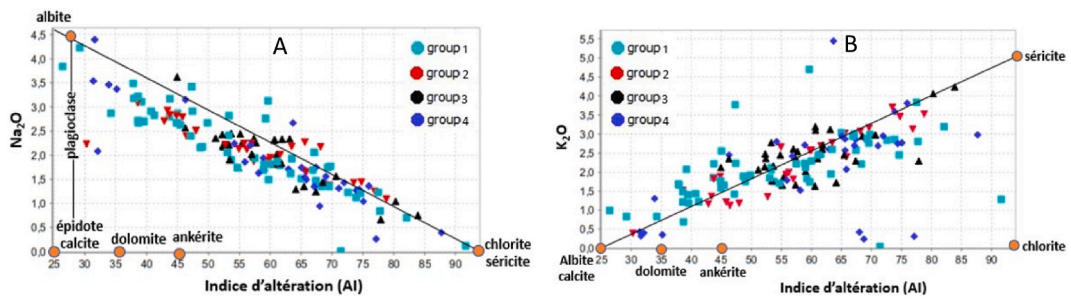


Fig. 9. Binary plots showing AI alteration trends with (A) Na<sub>2</sub>O and (B) K<sub>2</sub>O in metasedimentary rocks hosting the Boundiali gold prospect.

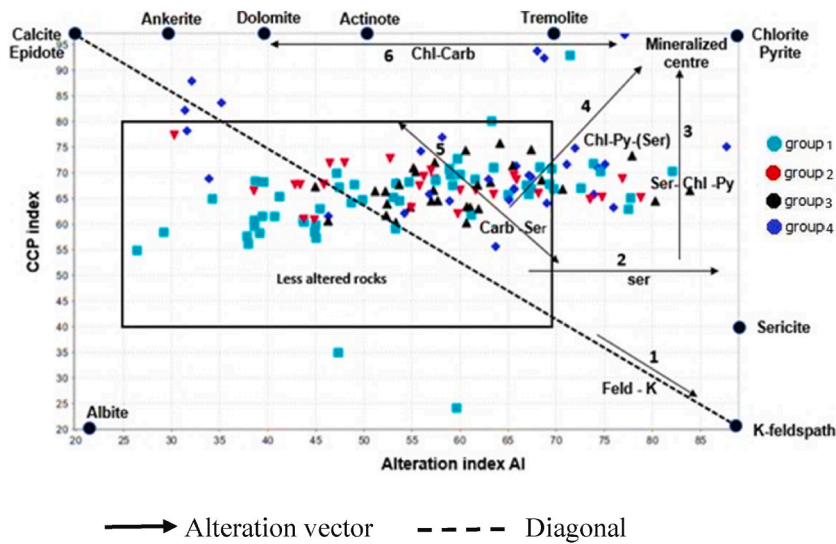


Fig. 10. Box plot binary alteration diagram [50] applied to samples of metasedimentary rocks hosting the Nyangoubé gold prospect.

in the metasediments, respectively. Those following the vector 6 trend are intensely altered to chlorite-carbonates (Fig. 10). Samples following the alteration vector 1 trend are in turn affected by intense potassic alteration. The box plot is designed in this study as a litho-geochemical study technique to estimate the intensity of hydrothermal alteration in the different groups of metasedimentary rocks hosting the gold mineralization of the Nyangoubé prospect and to place the samples of these groups in a context of mineralogical zonation revealed by the hydrothermal systems.

The assessment and quantification of hydrothermal alteration with all the geochemical relationships illustrated in the paragraphs above are all based on the movement of major elements, this implies that an increase in MgO in the metasedimentary rocks studied does not necessarily relate to an absolute gain in MgO [51,52]. To get a good picture of the movements of chemical elements during hydrothermal alteration, it is then convenient to calculate mass balances.

4.1.4. Mass balance

The mass balance assessment in this study is used to quantify and correlate hydrothermal alteration based on the chemistry of the metasedimentary facies hosting the mineralization.

The results of the mass balance calculations are presented in Figs. 11 and 12 as box plots. They present mass gains and losses for different groups of metasedimentary rocks (groups 1, 2, 3 and 4) distinguished hosting the gold mineralization at the Nyangoubé prospect. Elements such as SiO<sub>2</sub>, Na<sub>2</sub>O, K<sub>2</sub>O, CaO and Fe<sub>2</sub>O<sub>3</sub> represent alterations such as silicification, albitization, sericitization, carbonation and chlotization, respectively. The metasedimentary rocks recorded a Na<sub>2</sub>O mass balance ranging from -2.8 to +4 (Fig. 10). The majority of these rocks indicated a strong gain in Na<sub>2</sub>O related to a loss of K<sub>2</sub>O (-2.8). This increase in the mass of this element in the metasedimentary rocks could thus be due to an external contribution during hydrothermalism or to a sodium replacement in the networks of plagioclase phenocrysts. This gain in the mass of Na<sub>2</sub>O is therefore associated with the phenomenon of albitization during hydrothermal alteration. CaO was slightly enriched in some metasediment samples and slightly depleted in others. The enrichment of CaO in the metasediments is explained by the destruction of plagioclases with the neoformation of carbonates (calcite, ankerite and dolomite) and or due to the presence of quartz-carbonate veinlets. The loss of CaO during alteration may suggest that the calcium concentration was controlled by the replacement of calcium plagioclase and not by the presence of hydrothermal

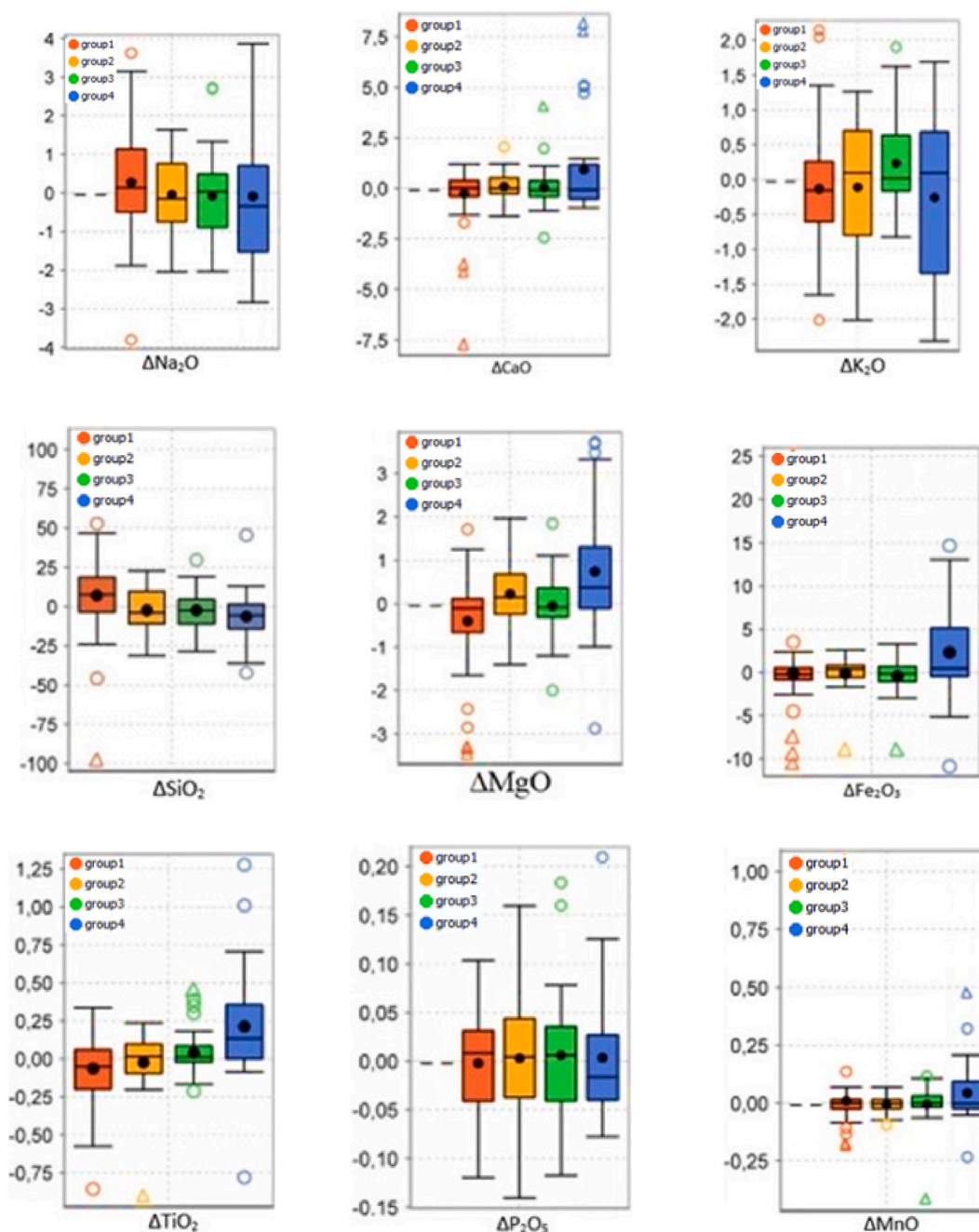


**Fig. 11.** Box plot showing mass changes during hydrothermal alteration for selected major elements in metasedimentary rocks hosting the Boundiali gold mineralization. Box plots are used to illustrate the mean (dot), median (line in the box) and scatter of the results. A box represents 50% of the values, two quantiles (the 25th and 75th percentiles). The lines attached to the boxes represent the 10th and 90th percentiles. The values that fall outside of the boxes are removed.

minerals with calcium. This could also be due to the replacement of calcium-rich primary hornblende by secondary biotite. Mass gains in CaO and Na<sub>2</sub>O, and in some cases, losses of these elements occur in rocks concentrating carbonates (calcite) and sodium feldspars (albite). These minerals (albite and calcite) are therefore abundant in metasediments with Na<sub>2</sub>O and CaO gain. The greater mass losses of Na<sub>2</sub>O and CaO in samples from the metasedimentary rocks in groups generally occur above and near the ore bodies. These losses express almost the destruction of sodium and calcium in these rocks. Larger mass gains in K<sub>2</sub>O were obtained in some of the metasediments in groups 3 and 4 (Fig. 11). All metasedimentary rock samples with K<sub>2</sub>O mass gain are mainly enriched in potassium feldspar, sericite, biotite, and micaceous clay minerals (illite), and are depleted in Na<sub>2</sub>O, CaO and SiO<sub>2</sub>. The increase of potassium in

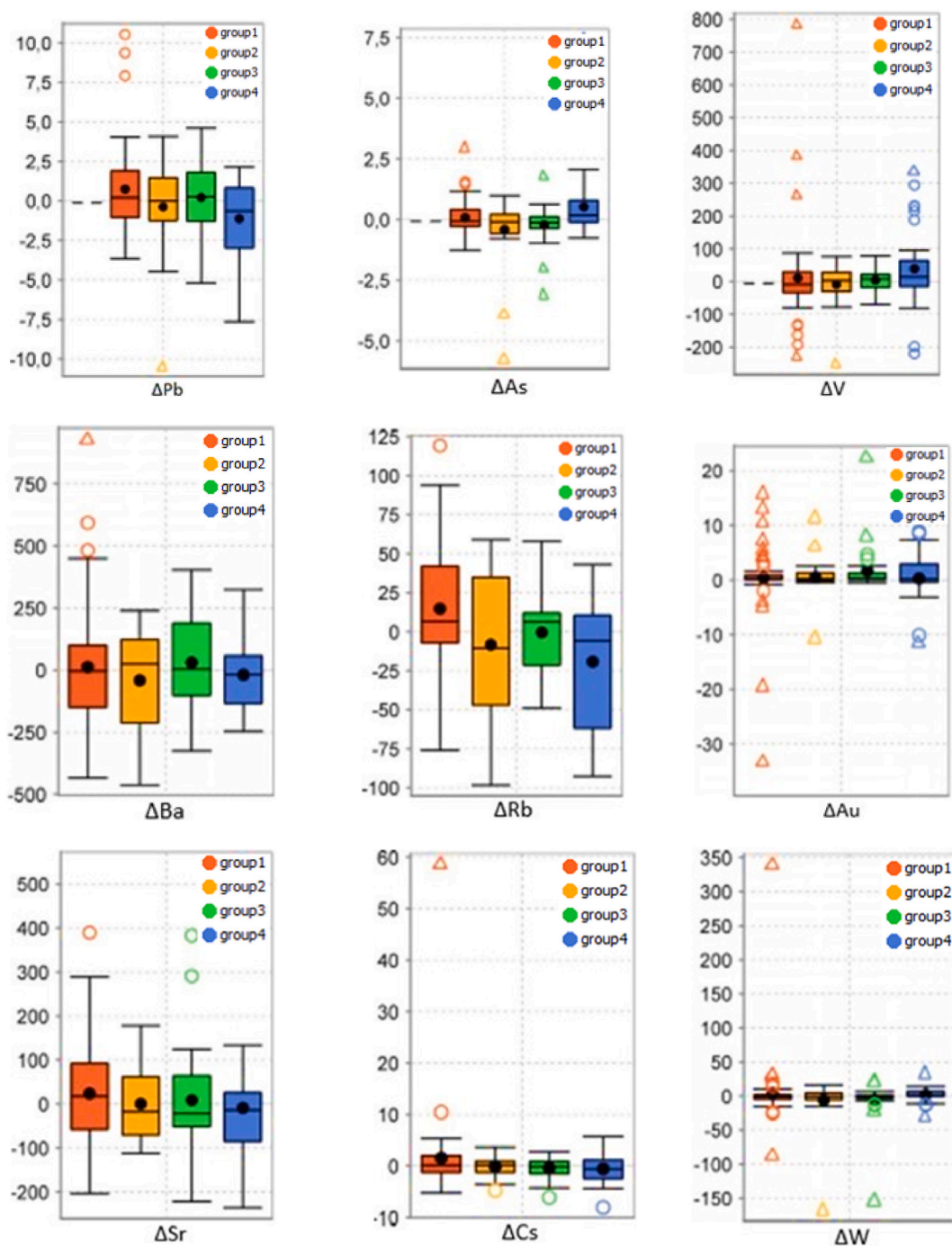


**Fig. 12.** Box plot illustrating mass changes produced during hydrothermal alteration for selected trace elements in metasedimentary rocks hosting the Boundiali gold mineralization. Box plots are used to illustrate the mean (dot), median (line in the box) and scatter of the results. A box represents 50% of the values, two quantiles (the 25th and 75th percentiles). The lines attached to the boxes represent the 10th and 90th percentiles. The values that fall outside of the boxes are removed.

the rocks affected by hydrothermal alteration is however explained by a replacement of plagioclase by sericite or biotite. This gain in potassium is therefore associated with the phenomenon of sericitization. Under these conditions, CaO is lost in response to the destruction of plagioclase, but the recorded gains would be caused by the development of quartz-carbonate veinlets in the metasedimentary rocks. Phosphorus ( $\text{P}_2\text{O}_5$ ), manganese ( $\text{MnO}$ ), titanium ( $\text{TiO}_2$ ) and iron ( $\text{Fe}_2\text{O}_3$ ) in metasedimentary rocks show limited mass changes due to fluid-rock interaction. Manganese was depleted in the metasedimentary rocks (Fig. 11), with samples in which it

was enriched containing chlorite richness in particular. Phosphorus loss reflects the degradation of phosphorus-rich minerals. The considerable addition of  $\text{SiO}_2$  in the metasediments is characterized by silicic alteration leading to a loss of  $\text{P}_2\text{O}_5$  and  $\text{CaO}$ . This results from the fact that quartz has replaced the primary and secondary minerals of igneous rocks contained in the metasedimentary rocks [48]. Samples from the metasedimentary groups with the largest silicon gains usually occur close to gold mineralization.

It is noted that  $\text{TiO}_2$  and  $\text{Fe}_2\text{O}_3$  experienced a significant mass gain in some samples from different metasedimentary groups. This could be explained by the destabilization of amphiboles (hornblende) by hydrothermal fluids charged with Mn, Fe and Ti. The interaction between these fluids and the source rocks of the hornblende-rich metasedimentary rocks would produce an exchange of elements such as Na, Al, and Ca and probably the formation of  $\text{Fe}_2\text{O}_3$ , MnO and  $\text{TiO}_2$ . These exchanges could mark the presence of clay and sericite minerals in these metasedimentary group samples. The addition of iron is due to the dissemination of pyrite and chalcopyrite minerals in the metasedimentary rocks and the development of chlorite minerals. We also note an enrichment of certain samples in metallic elements such as Pb, W, As and V (Fig. 12). The increase in mass changes of Cs, Ba, and Rb in the metasediments is due to the destabilization of potassium feldspars and neoformation of sericite (Fig. 12). Cs, Ba and Rb thus coexist with K in the potassium feldspars. We note that the enrichment of the samples in Rb and K occurs with the development of potassic micas and potassic feldspars during the potassic metasomatic process. The mass in Rb increases with the increase of  $\text{K}_2\text{O}$ . This is related to an abundance of secondary biotite in the metasedimentary rocks [53].

The loss of Rb in the samples combines with the phenomena of argillization and silicification and/or the formation of chlorite. The

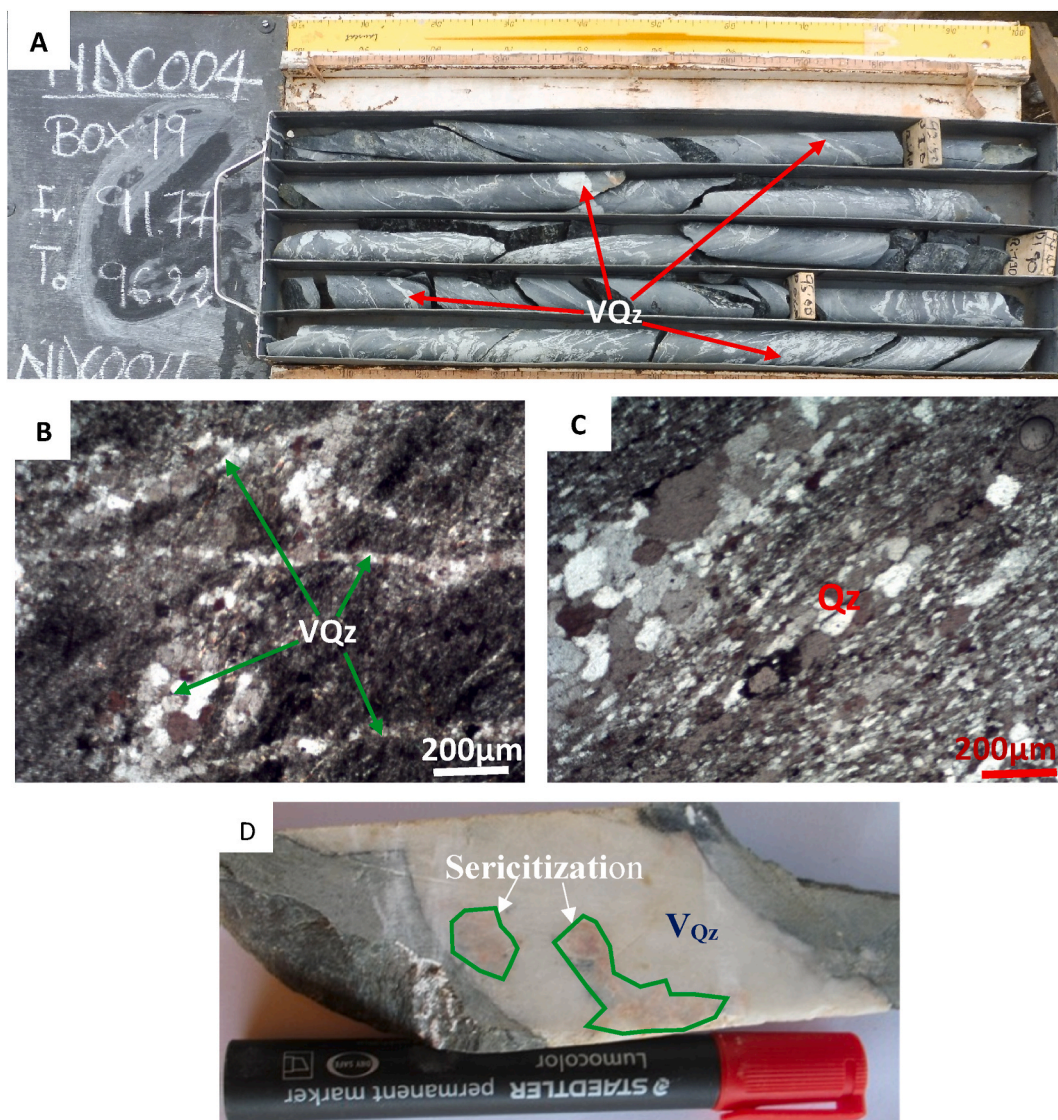


**Fig. 13.** Photographs (A, D) and microphotographs (B, C) of silicification-associated alteration assemblages. A) quartz veinlet network on cores, B) quartz-carbonate veinlet network in thin slide, C) thin slide showing dissemination of quartz grains in metasedimentary rocks, D) quartz vein overprinting sericitization. VQz: quartz veinlet, Qz: quartz.

highly mobile trace elements Sr and V are the first trace elements following  $\text{Na}_2\text{O}$ , CaO and MgO in their mobility in the formation of hydrothermal minerals. The depletion of strontium and barium would be caused by the degradation of primary potassium feldspar, plagioclase, and sericite. Hydrothermally altered metasedimentary groups show a significant gain in Au, W, V, As and Pb concentration (Fig. 12).

The metasediments show a moderate in Au, reflecting the dissemination of pyrite and chalcopyrite in them. The definition of alterations and the determination of mass exchanges of chemical elements can be very useful in the definition of exploration vectors.

#### 4.2. Mineralogy of hydrothermal alteration assemblages

The mineralogical study of the alteration assemblages identifies changes in the primary mineralogy of the metasedimentary rocks hosting the gold mineralization at the Nyangoubé prospect and indicator minerals that characterize the proximity to the mineralization. This study describes the different mineralogical manifestations related to the impregnated alterations in the gold-bearing lens based on the results of petrographic descriptions. The types of hydrothermal alteration associated with gold mineralization at the Nyangoubé prospect are varied and included carbonation, sericitization, silicification, biotitization, sulfidation, chloritization and albitization.

##### 4.2.1. Silicification

Silicification is a type of hydrothermal alteration referring to the neoformation of quartz or silica in rocks during weathering. It is a process of integration of silica in the surrounding lithologies during hydrothermal and magmatic phenomena and during the migration and precipitation of silica in sedimentary rocks [54]. Observations from drill cores and microscopy show that silicification affects almost all lithologies (Fig. 13A–D). The silicification phenomenon appears in two forms:

- the first form corresponds to a vein alteration phase where the hydrothermal fluids enriched in gold and metals partially clog the quartz and carbonate fractures as they pass through to form veins or veinlets (Fig. 13A, D). In this form, its phase is marked by a

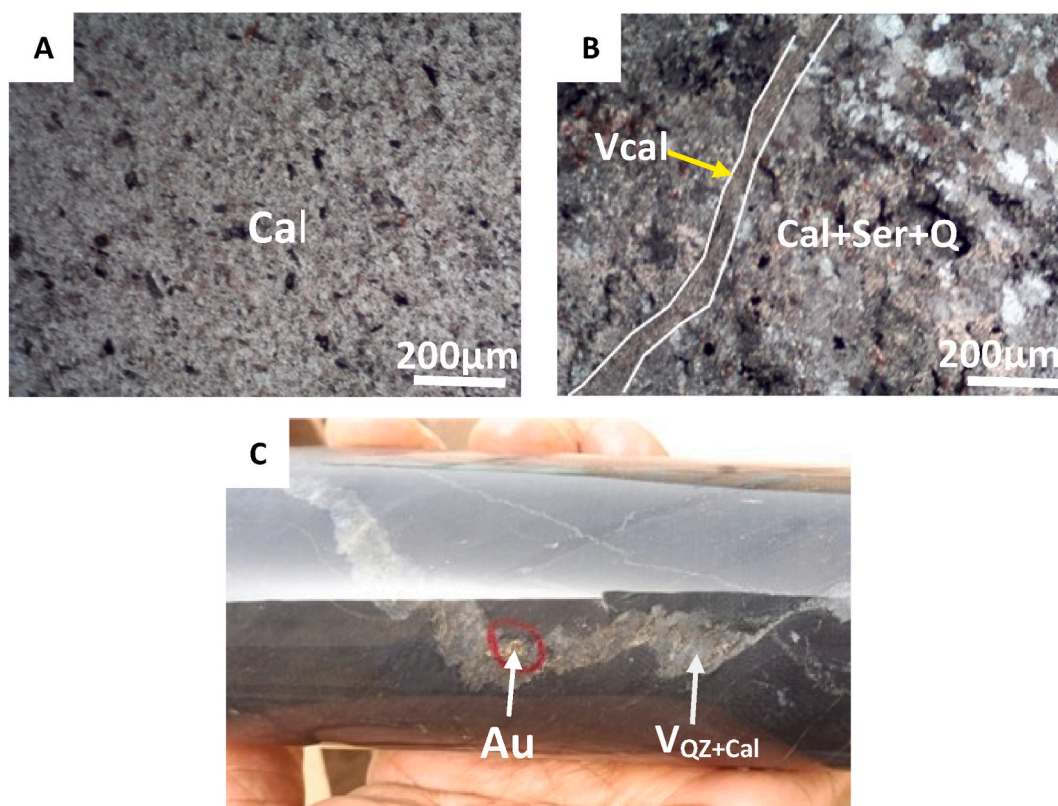


**Fig. 14.** Microphotographs (A, B) and photograph (C) of alteration assemblage associated with carbonation. A) destruction of feldspars in place of carbonate (calcite); B) thin slide showing a carbonate veinlet intersecting the carbonate (calcite) dominated rock matrix; C) mineralized quartz-carbonate vein.  $V_{Qz}$ : quartz veinlet, Qz: quartz,  $V_{Qz} + \text{Cal}$ : mineralized quartz-carbonate vein,  $V_{\text{Cal}}$ : calcite veinlet, Cal: calcite, Ser: sericite, Au: gold.

network of quartz veinlets (Fig. 13B). Silicon is commonly derived from the leaching of the surrounding rocks through which these fluids flow.

- the second form corresponds to a dissemination alteration during which the hydrothermal fluids circulate through the permeable surrounding rocks while clogging the latter during their crossing. Quartz occurs in the diffuse form in the rocks and not in vein form (Fig. 13C).

Silicification could be synchronous with carbonation and sulfidation because many silicified lithologies include sulfide and carbonate (calcite, dolomite or ankerite) veins and veinlets. The silicification is intense and induces the replacement of the primary minerals by quartz. Sulfides and sericite precipitate weakly with secondary quartz in the metasedimentary rocks. The silicified metasedimentary rocks are affected by ductile deformation stretching the secondary quartz minerals along the plane of the schistosity.

#### 4.2.2. Carbonation

Carbonation is characterized by the addition of carbonates at the expense of plagioclases and alkali feldspars during the alteration of rocks. Carbonation has affected the entire metasedimentary lithology hosting the gold mineralization at the Nyangoubé prospect. It is characterized by a predominance of calcite and to a lesser degree by dolomite and/or ankerite then incidentally by sericite and quartz. In thin sections, carbonates are found in the surrounding rocks in diffuse and penetrative form (Fig. 14A and B) and constitute the vein-filling material (Fig. 14B). Calcite remains the carbonate mineral of the quartz gangue, which is well-represented in the thin sections. Carbonation is temporally related to gold mineralization and is synchronous with silicification. These two alteration processes are synchronous with the precipitation and crystallization of gold in mineralized veins and veinlets (Fig. 14C). Carbonation is therefore considered a precursor event to gold mineralization [13]. It is a process of hydrothermal alteration generating a gain in the mass of the surrounding rocks.

#### 4.2.3. Sericitization

Sericitization is an alteration process related to the destabilization of potassium plagioclase and biotite to form sericite (fine-grained mica). This alteration affects almost all of the mineralization's host formations and is one of the most dominant pervasive alterations in the study area. In thin sections, sericite appears as reddish, yellowish or bluish flakes oriented along the schistosity planes (Fig. 15 A, B). It would come either from the alteration of primary minerals (biotite and potassic plagioclases) or the neoformation from greenschist metamorphism. However, the sericite developed in the mineralization zones is of hydrothermal origin. It combines with carbonates and chlorite to form the rock matrix. Sulfide minerals are ubiquitous in small quantities, in the disseminated form and in the sericitization assemblages.

#### 4.2.4. Chloritization

Chloritization is a none pervasive alteration in the study area but to a regional extent. It is characterized by a partial or total alteration of some clayey minerals, biotite, pyroxene and amphibole crystals. Chlorite identified in the surrounding formations of the Nyangoubé prospect gold mineralization occurs as thin greenish patches (Fig. 16). It is part of the chlorite-sericite-epidote-amphibole-calcite  $\pm$  quartz assemblage. With increasing intensity of deformation, the chlorite is oriented along the direction of the schistosity (Fig. 16A and B). When the intensity of deformation is low, the chlorite minerals have no preferential orientation (Fig. 16 C, D). They are minerals accompanying the mineralization in association with sericite in the formation of a micaceous matrix of the surrounding rocks.

#### 4.2.5. Sulfidation

Sulfidation is a process of sulfide formation by the addition of sulfur that increases the proportions of sulfide minerals in rocks. In

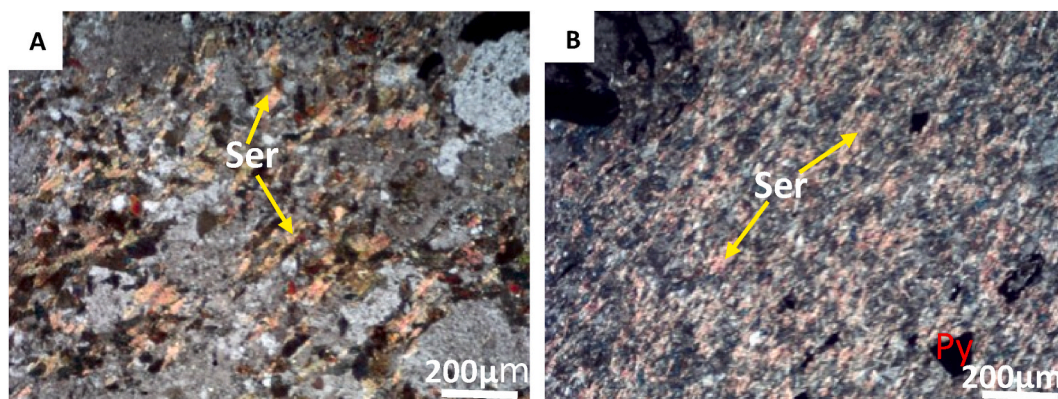


**Fig. 15.** Microphotographs of alteration assemblages associated with sericitization. A: Sericite locally replacing plagioclase; B: total replacement of plagioclase by sericite with the dissemination of pyrite.

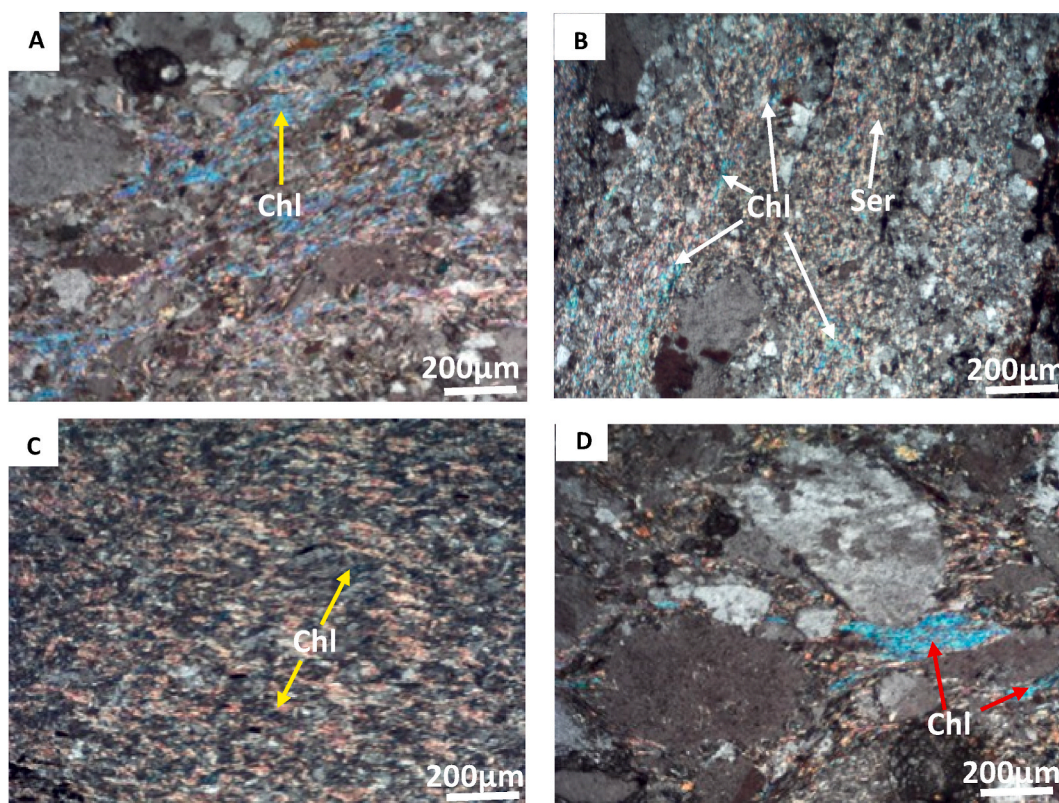


**Fig. 16.** Microphotographs of alteration assemblages associated with chloritization. A, B: chlorite-dominated laminae along the direction of schistosity; C, D: disoriented chlorite in metasediments.

the Nyangoubé gold prospect, sulfidation is marked by the development of pyrite, arsenopyrite and chalcopyrite. These sulphides are developed in the host rocks of the mineralization in a disseminated manner constituting porphyroblasts of the rock matrix (Fig. 17B, C, D) and veinlets intersecting the rock matrix (Fig. 17A). Sulphidation is an alteration process, usually, post to late metamorphic, that results in the remobilization of some sulphides and the emplacement of others that may be related to gold mineralization. The sulphides are hydrothermal and their presence is directly related to gold mineralization. Near the mineralized zones, the intensity of the deformation increases and the sulphides orient themselves in the direction of the schistosity (Fig. 17D).

## 5. Discussion

The classification of metasediments into four groups based on  $\text{Al}_2\text{O}_3/\text{TiO}_2$  ratios suggests that these rocks have different sources of provenance [42]. A significant number of samples from these distinguished rock groups appear to contain higher  $\text{Na}_2\text{O}$  content, suggesting an external input of sodium, which may be responsible for the formation of secondary albite. The same observation was also found in the case of  $\text{K}_2\text{O}$ , this supposes an external contribution of potassium favoring the formation of sericite or secondary biotite [48, 55]. A good number of samples of group 4 metasediments seem to have significant  $\text{MgO}$  contents suggesting an external contribution of magnesium in these samples and a development of chlorite.

The ternary diagrams constructed from the major elements of the host rocks indicate that the hydrothermal alteration vectors associated with the mineralization are dominated by sericitization and chloritization. These vectors illustrate the influence of hydrothermal alteration on the chemical composition of the metasedimentary rocks hosting the gold mineralization. These have significantly higher potassium, magnesium, and iron contents. Potassic alteration, therefore, represents the type of hydrothermal alteration that predominates in the prospect. The addition of  $\text{K}_2\text{O}$  and  $\text{Na}_2\text{O}$  during the formation of silicate minerals is restricted by the availability of  $\text{Al}_2\text{O}_3$ , which is why the  $\text{K}_2\text{O}/\text{Al}_2\text{O}_3$  and  $\text{Na}_2\text{O}/\text{Al}_2\text{O}_3$  molar ratios are therefore considered to be good vectors for measuring the intensity of the formation, sericitization and albitization [56–59]. The  $\text{K}_2\text{O}/\text{Al}_2\text{O}_3$  ratios vary depending on the sericite content in the metasedimentary rocks. This implies that these metasediments were affected by strong (proximal and distal) potassium and sodium weathering. Under these conditions, the samples from the metasedimentary groups are enriched in  $\text{K}_2\text{O}$  and  $\text{Na}_2\text{O}$  and depleted in  $\text{MgO}$ . Low  $\text{K}_2\text{O}/\text{Al}_2\text{O}_3$  ratios determine the mineralogical assemblage associated with mineralization [60,61]. This mineralogical assemblage is composed of quartz-carbonate-micas (sericite and biotite)-pyrite-chlorite-albite. The mineralized areas of the study area are then distinguished by an increase in the  $\text{K}_2\text{O}/\text{Al}_2\text{O}_3$  ratios as well as the gold grades. As for the  $\text{Na}_2\text{O}/\text{Al}_2\text{O}_3$  ratios, high values characterize areas with high albite proportions. These zones are therefore indicators of the potential mineralogical



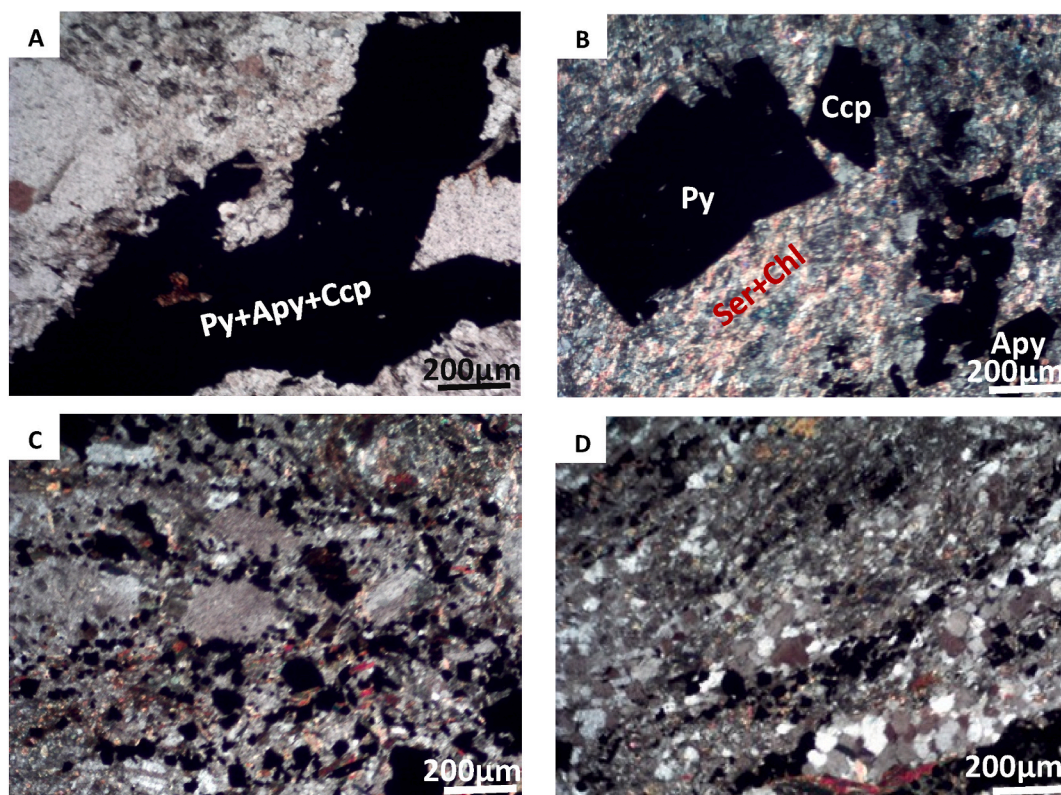


**Fig. 17.** Microphotographs of alteration assemblages associated with sulfidation. A) sulfide veinlet (pyrite, arsenopyrite and chalcopyrite) intersecting the rock matrix, B) gaining surficial porphyroblasts in a sericite-chlorite matrix; C) dissemination of disoriented sulfides due to low-intensity of deformation; D) sulfurs disseminated in metasediments and oriented in the direction of schistosity. Ser: sericite, Chl: chlorite, Py: pyrite, Apy: arsenopyrite, Ccp: chalcopyrite.

ensemble in the mineralized areas. The obtained  $\text{Na}_2\text{O}/\text{Al}_2\text{O}_3$  molar ratios are highly variable and show an antithetical relationship with the sericite saturation index. This would be due to sodium leaching associated with the destruction of metamorphic albite and hydrothermal plagioclase [48,62]. The decrease in the albite saturation index suggests a decrease in the amount of feldspar in the hydrothermally altered metasedimentary rocks. It then had a weak albitization reaction, therefore a non-pervasive albitic alteration.  $(\text{K}_2\text{O} + \text{Na}_2\text{O})/\text{Al}_2\text{O}_3$  ratios vary depending on the intensity of sericite and albite saturation. The evolution of these ratios indicates that the zones of gold mineralization have been affected by a strong potassic alteration called pervasive and a weak sodic not pervasive alteration. Under these conditions, the samples of the metasedimentary groups are then enriched in  $\text{K}_2\text{O}$  and  $\text{Na}_2\text{O}$  and depleted in  $\text{MgO}$ . Metasedimentary rocks with higher AI and CCP weathering indices are affected by chloritization, sericitization and silicification processes caused by mass transfer during a hydrothermal system [59,61,63]. Those with moderately high AI and CCP alteration indices are dominated in their mineral paragenesis by pyrite, carbonates and chlorite resulting from hydrothermal alteration [64,65]. The alteration vectors discriminated from the diagram of Large et al. [50] suggest that the gold mineralization of the Nyangoube prospect was affected by different episodes of hydrothermal alteration. To specify these alterations, a calculation of the mass balance per single precursor was applied.  $\text{Na}_2\text{O}$  enrichment of the metasediments suggests that much of the sodium involved in the replacement of calcium plagioclases by albite is derived locally and may have been released during the replacement of oligoclase by microcline [66]. The albitization footprints are found everywhere within the metasedimentary rocks hosting the mineralization. It increases markedly at the walls of mineralized quartz and quartz-carbonate veins oriented NNE-SSW [67]. The  $\text{CaO}$  was enriched only weakly in the metasedimentary rocks during the alteration, this shows that the calcium of the carbonates would come from the decomposition of calcium plagioclases in albite. The hydrothermal alteration of the metasedimentary rocks is therefore marked by a progressive conversion of plagioclase by microcline and albite. The enrichment of metasedimentary rocks in  $\text{Fe}_2\text{O}_3$  and  $\text{K}_2\text{O}$  is manifested by the mineralogical coupling between sulphidation and potassium alteration processes [68,69].  $\text{Fe}_2\text{O}_3$  gains could also be caused by the hematization of less-weathered precursor rocks used in the assessment of mass balances. The phenomenon of albitization assisted by hematization during hydrothermal alterations is therefore typical of the alkaline metasomatic phenomenon known as fenitization [70]. Fenitization is particularly linked to carbonatitic and alkaline complexes. It has been described in the Lac Shortt mine and proposed as a possible regional auriferous metallogenic [71,72]. The enrichment in  $\text{SiO}_2$ ,  $\text{K}_2\text{O}$ ,  $\text{Na}_2\text{O}$  and  $\text{CaO}$  as well as the losses in  $\text{MgO}$  and  $\text{Fe}_2\text{O}_3$  are then characteristic of the zones of mineralization [48,73]. These analytical results are in agreement with the mineralogy of the hydrothermal alterations identified in the thin section and express a new apparent alkaline mineralogy. These

remarks inform us that the whole of the alteration was controlled more by the composition of the metasedimentary rocks hosting the gold mineralization. All of the metasedimentary facies surrounding the Nyangoubé gold prospect are affected by fissural and pervasive alteration marking the extent of the hydrothermal alteration of this prospect. The mineralogical assemblage marking the proximal pervasive alteration is highly varied. These minerals are therefore produced during various alterations such as silicification, carbonation, sericitization, sulphidation and biotitization, chloritization and to one-degree albitization. These alteration vectors corroborate those revealed by hydrothermal alteration geochemistry in this study.

Silicification in the metasediments being marked by the development of networks of quartz veinlets and disseminated quartz grains suggests the interaction between hydrothermal fluids and these rocks. It is explained by the addition or replacement of quartz to the detriment of the minerals existing in the rocks at the contact between fluids and rocks. When hydrothermal fluids carrying dissolved gold react with host rocks, silicification occurs concurrently with gold concentration [74,75]. Gold can be precipitated directly in quartz as a gold-bearing mineral like auriferous pyrite. This phenomenon corroborates with the geochemical data expressing a mass gain of SiO<sub>2</sub> in the metasedimentary rocks. Gold can be precipitated directly in quartz as a gold-bearing mineral like auriferous pyrite. This phenomenon corroborates with the geochemical data expressing a mass gain of SiO<sub>2</sub> in the metasedimentary rocks.

Sulphidation in metasediments involves a considerable addition of sulfur, which particularly associates with Cu, Fe, Zr and Pb to form complexes capable of transporting Au through hydrothermal fluids that interact with these rocks [76–78]. This range of alteration affecting the metasedimentary rocks suggests the great compositional diversity of the lithologic facies hosting the gold mineralization and the variation in the chemistry of the mineralizing fluids.

## 6. Conclusion and implication for mining exploration

The results of hydrothermal alteration studies using rock geochemical and petrographic data are compelling tools for mapping the intensity and distribution of fluid-rock interaction related to gold mineralization. Hydrothermal alteration related to mineralization systems generally induces the destruction of plagioclase in the studied metasediments and their replacement by sericite, chlorite, carbonates, quartz, and sulfides in variable proportions depending on the intensity of each type of alteration associated with the formation of each mineral. The mass gains in elements such as SiO<sub>2</sub>, Na<sub>2</sub>O, K<sub>2</sub>O, CaO and Fe<sub>2</sub>O<sub>3</sub> are respectively indicative of alterations such as silicification, albitization, sericitization, carbonation and chloritization which are the different types of hydrothermal alterations associated with the mineralization of the study area. Using the whisker box, it is possible to distinguish between less altered and hydrothermally altered samples. Four different mineralogical trends related to hydrothermal alteration associated with mineralization in the study area were defined in the whisker box.

Petrographic studies of the paragenetic relationships of hydrothermal alteration minerals are important to maximize the utility of total rock geochemical data. The diversity of hydrothermal minerals identified reflects a great compositional heterogeneity of the lithologies hosting the gold mineralization and variability in the chemistry of the mineralizing fluids. For exploration, it is important to identify the intensity gradients of potassium metasomatism and the vectors of hydrothermal alteration in prospective areas. Vectors will exist in areas where hydrothermal alteration is zoned around structural features that concentrate hydrothermal fluids favourable for gold mineralization. In this context, shear zones, faults and N–S to NNE–SSW trending lithological contacts that are ductile-breakable deformation structures are hydrothermal drains of gold-bearing fluids. Mineralogical assemblages such as sericite-chlorite-pyrite, chlorite-pyrite±sericite, carbonate-sericite and chlorite-carbonate revealed by hydrothermal alteration trends in the host rocks could also help to identify potential gold corridors in the study area and its peripheries. The results of the mass balance calculations show a progressive increase in the concentration of Au, W, V, As and Pb as well as K<sub>2</sub>O, CaO, Na<sub>2</sub>O and Fe<sub>2</sub>O<sub>3</sub>, which could be vectoring parameters towards gold mineralization. This geochemical signature could potentially be applied in gold exploration.

### Author contribution statement

Lipoubliida Djagre: Conceived and designed the experiment; Performed the experiments; Analyzed and interpreted the data; Wrote the paper.

Barthélémy Gnammytchet Koffi and Moussa Camara: Conceived and designed the experiment; Contributed reagents, materials, analysis tools or data.

Gbele Ouattara and Yao Agbossoumonde: Conceived and designed the experiments.

### Data availability statement

Data will be made available on request.

### Declaration of competing interest

The authors declare that they have no known competing financial interests or personal relationships that could have appeared to influence the work reported in this paper.

### Acknowledgements

We would like to express our gratitude to the African Center of Excellence Mines and Mining Environment for their financial

support for this research, as well as to the mining company Turaco Gold for generously making part of the geochemical data used in this study available to us.

## References

- [1] É.L. Mignot, Les gisements d'or comme témoins de l'histoire géologique du craton ouest-africain: apports de la datation, 2014, p. 340.
- [2] S.M. Elatikpo, H. Li, H. Zheng, M.B. Girei, J. Wu, A.K. Amuda, Cryogenian crustal evolution in western Nigeria shield: whole-rock geochemistry, Sr-Nd and zircon U-Pb-Hf isotopic evidence from Bakoshi-Gadanya granites, *Int. Geol. Rev.* 64 (2022) 2626–2652, <https://doi.org/10.1080/00206814.2021.1998799>.
- [3] S.M. Elatikpo, H. Li, B. Liu, W.D. Zhang, Metallogenesis of the Bakoshi-Kundila gold deposit in northern West Nigerian Subshield: insights from pyrite chemical and sulfur isotopic compositions and zircon U-Pb geochronology, *Precambrian Res.* 383 (2022), 106890, <https://doi.org/10.1016/j.precamres.2022.106890>.
- [4] M. Elatikpo, H. Li, C. Yuanlin, H. Abba Ahmed, Genesis and magma fertility of gold associated high-K granites: LA-ICP-MS zircon trace element and REEs constraint from Bakoshi-Gadanya granites in NW Nigeria, *Acta Geochimica* 41 (2022), <https://doi.org/10.1007/s11631-022-00528-z>.
- [5] D.I. Groves, R.J. Goldfarb, F. Robert, C.J.R. Hart, Gold deposits in metamorphic belts: overview of current understanding, outstanding problems, future research, and exploration significance, *Econ. Geol.* 98 (2003) 1–29.
- [6] D.I. Groves, R.J. Goldfarb, F. Robert, C.J.R. Hart, Gold deposits in metamorphic belts: overview of current understanding, outstanding problems, future research, and exploration significance, *Econ. Geol.* 98 (2003) 1–29.
- [7] J.-P. Milési, Minéralisations aurifères de l'Afrique de l'ouest leurs relations avec l'évolution lithostructurale au Proterozoïque inférieur, 1989.
- [8] P.K. Eilu, C. Mathison, D. Groves, W. Allardye, Atlas of Alteration Assemblages, Styles and Zoning in Orogenic Lode-Gold Deposits in a Variety of Host Rock and Metamorphic Settings, Geology & Geophysics Department (Centre for Strategic Mineral Deposits) & UWA Extension, The University of Western Austr, Perth, 1999.
- [9] M. Jébrak, E. Marcoux, Géologie des ressources minérales, Ministère des ressources naturelles et de la faune, Québec, 2008.
- [10] J. Dubé, Caractérisation métallogénique et structurale de la minéralisation aurifère des gisements Triangle et Cheminée No. 4, Val-d'Or, Abitibi, Québec, 2018, p. 259.
- [11] Z. Ouattara, Y. Coulibaly, pétrographie du gisement d'or de Bonikro, sillon birimien d'Oumé - fettékro, Côte d'Ivoire, 2015, p. 14.
- [12] K.E. Assie, Lode Gold Mineralization in the Paleoproterozoic (Birimian) Volcano-Sedimentary Sequence of Afema Gold District, southeastern Côte d'Ivoire, 2008, p. 198.
- [13] H.N. Nestor, Etude pétrologique, structurale et métallogénique du gisement aurifère d'Agbahou, Divo, Côte d'Ivoire, 2013.
- [14] A. Gnanzou, Étude des séries volcano-sédimentaires de la région de Dabakala (Nord-Est de la Côte d'Ivoire): genèse et évolution magmatique : contribution à la connaissance de la minéralisation aurifère de Bobosso dans la série de la Haute-Comoé, 2014, p. 304.
- [15] K.B.K. Pothin, P. Gioan, C.C. Gronayes, Bilan géochronologique du socle précambrien de Côte d'Ivoire, Bioterre, Revue Internationale Des Sciences de La Vie et de La Terre 1 (2000) 36–47.
- [16] B. Bessoles, géologie de l'Afrique. Le craton ouest africain, 1977.
- [17] o. gbele, structure du batholite de ferkessedougou (secteur de zuenoula, côte d'ivoire): implications sur l'interpretation de la geodynamique du paleoproterozoïque d'afrique de l'ouest a 2.1 ga, 1998, p. 344.
- [18] A.-N. Kouamelan, Géochronologie et Géochimie des Formations Archéennes et Protérozoïques de la Dorsale de Man en Côte d'Ivoire. Implications pour la Transition Archéen-Protérozoïque, 1996, p. 319.
- [19] D.A. Wood, The application of a ThHfTa diagram to problems of tectonomagmatic classification and to establishing the nature of crustal contamination of basaltic lavas of the British Tertiary Volcanic Province, *Earth Planet Sci. Lett.* 50 (1980) 11–30, [https://doi.org/10.1016/0012-821X\(80\)90116-8](https://doi.org/10.1016/0012-821X(80)90116-8).
- [20] Legoux, Le massif de Man (Côte d'Ivoire), Essai de géologie pétrographique, by, in: P. LEGOUX (Ed.), Bon Etat Couverture Souple, 1939.
- [21] J. Camil, I. Yace, J.-P. Tastet, B. Toure, M. Roques, D. Demaiffe, T. Tempier, Pétrographie, chronologie des ensembles granulitiques archéens et formations associées de la région de Man (Côte d'Ivoire), 1984. <https://invenio1.uvci.edu.ci/record/7939/>. (Accessed 19 February 2022).
- [22] I. Yacé, The Precambrian of West Africa and its Correlation with Eastern Brazil, PIGC Final Report, CIFEG Paris, Publ. Occas., 1984, p. 28.
- [23] B. Tagini, Esquisse structurale de la Côte d'Ivoire. Essai de geotectonique regionale, These Univ. Lausanne. Societe d'Etat Pour Le Developpement Miniere de La Cote D'Ivoire, 1971. <https://cir.nii.ac.jp/crid/1572543024963374208>. (Accessed 27 February 2023).
- [24] J.-L. Feybesse, J.-P. Milési, The Archaean/Proterozoic contact zone in West Africa: a mountain belt of décollement thrusting and folding on a continental margin related to 2.1 Ga convergence of Archaean cratons? *Precambrian Res.* 69 (1994) 199–227, [https://doi.org/10.1016/0301-9268\(94\)90087-6](https://doi.org/10.1016/0301-9268(94)90087-6).
- [25] S. Lemoine, évolution géologique de la région de Dabakala (NE de la Côte d'Ivoire) au Protérozoïque inférieur. Possibilités d'extension au reste de la Côte d'Ivoire et au Burkina Faso: similitudes et différences; les linéaments Greenville-Ferkessedougou et grand Cess-niakaramandougou, 1988 [s.n.].
- [26] A. Poucllet, S. Doumbia, M. Vidal, Geodynamic setting of the birimian volcanism in central ivory Coast (western Africa) and its place in the paleoproterozoic evolution of the man shield, *Bull. Soc. Geol. Fr.* 177 (2006) 105–121.
- [27] M.H. Leake, The Petrogenesis and Structural Evolution of the Early Proterozoic Fetekro Greenstone Belt, Dabakala Region, NE Cote D'Ivoire, PhD Thesis, University of Portsmouth, 1992.
- [28] B. Daouda Yao, Lithostratigraphie et petrologie des formations birimiennes du sillon de toumodi-fettékro (cote-d'ivoire) : implication pour l'evolution crustale du paleoproterozoïque du craton ouest-africain, These de doctorat, Orléans, 1998. <http://www.theses.fr/1998ORLE2034>. (Accessed 20 January 2021).
- [29] W. Hirdes, D.W. Davis, G. Lüdtke, G. Konan, Two generations of Birimian (Paleoproterozoic) volcanic belts in northeastern Côte d'Ivoire (West Africa): consequences for the 'Birimian controversy', *Precambrian Res.* 80 (1996) 173–191, [https://doi.org/10.1016/S0301-9268\(96\)00011-3](https://doi.org/10.1016/S0301-9268(96)00011-3).
- [30] C. Delor, M. Vidal, Z. Zead, Y. Koné, Notice explicative de la carte géologique de la Côte d'Ivoire au 1/200 000, feuille Nassian, 1995.
- [31] M. Vidal, C. Delor, A. Poucllet, Y. Simeon, G. Alric, Evolution géodynamique de l'Afrique de l'Ouest entre 2, 2 Ga et 2 Ga ; le style "archéen" des ceintures vertes et des ensembles sédimentaires birimiens du nord-est de la Côte-d'Ivoire, *Bull. Soc. Geol. Fr.* 167 (1996) 307–319.
- [32] K.A.Y. Yao, Le volcanisme du sillon de boundiali, phenomene principal du proterozoïque inferieur de cette region n-nw de la cote d'ivoire, These de doctorat, vol. 2, Clermont-Ferrand, 1993. <https://www.theses.fr/1993CLF21483>. (Accessed 31 August 2021).
- [33] P. Turner, Evolution of the Early Proterozoic Boundiali-Bagoe Supracrustal Belt and Associated Granitic Rocks, Northern Cote d'Ivoire, Ph.D., University of Portsmouth, West Africa, 1995.
- [34] J.P. Liégeois, W. Claessens, D. Camara, J. Klerkx, Short-lived Eburnian orogeny in southern Mali. Geology, tectonics, U-Pb and Rb-Sr geochronology, *Precambrian Res.* 50 (1991) 111–136, [https://doi.org/10.1016/0301-9268\(91\)90050-K](https://doi.org/10.1016/0301-9268(91)90050-K).
- [35] J.-L. Feybesse, J.-P. Milési, The Archaean/Proterozoic contact zone in West Africa: a mountain belt of décollement thrusting and folding on a continental margin related to 2.1 Ga convergence of Archaean cratons? *Precambrian Res.* 69 (1994) 199–227, [https://doi.org/10.1016/0301-9268\(94\)90087-6](https://doi.org/10.1016/0301-9268(94)90087-6).
- [36] J.-P. Milési, P. Ledru, J.-L. Feybesse, A. Dommanget, E. Marcoux, Early proterozoic ore deposits and tectonics of the birimian orogenic belt, west Africa, precambrian research - PRECAMBRIAN, RES 58 (1992) 305–344, [https://doi.org/10.1016/0301-9268\(92\)90123-6](https://doi.org/10.1016/0301-9268(92)90123-6).
- [37] M. Vidal, A. Prost, G. Alric, S. Lemoine, Présence d'un socle antérieur à une suture océanique du Birimien inférieur en Côte-d'Ivoire (Afrique de l'Ouest), *Comptes Rendus de l'Académie Des Sciences. Série 2, Mécanique, Physique, Chimie, Sciences de l'univers, Sciences de La Terre* 315 (1992) 193–200.
- [38] R. Couture, Carte géologique au 1/500000 feuille Odiné, Mines Géol. Abidjan, Abidjan, 1968.
- [39] A.G. Beaudou, R. Sayol, Etude pédologique de la région de Boundiali - Korhogo (Côte d'Ivoire) : cartographie et typologie sommaire des sols, feuille Boundiali, feuille Korhogo à 1/200, vol. 000, 1980, p. 58.
- [40] Daouda Yao, Adou M'bé, Simeon Yves, Carte géologique de la zone d'étude extraite de la feuille géologique de Boundiali à 1/200 000, 1995.
- [41] R.L. Gresens, Composition-volume relationships of metasomatism, *Chem. Geol.* 2 (1967) 47–65, [https://doi.org/10.1016/0009-2541\(67\)90004-6](https://doi.org/10.1016/0009-2541(67)90004-6).
- [42] P.W. Fralick, B.I. Kronberg, Geochemical discrimination of clastic sedimentary rock sources, *Sediment. Geol.* 113 (1997) 111–124, [https://doi.org/10.1016/S0037-0738\(97\)00049-3](https://doi.org/10.1016/S0037-0738(97)00049-3).

- [43] M. Michael, Herron, geochemical classification of terrigenous sands and shales from core or log data, *SEPM JSR* 58 (1988), <https://doi.org/10.1306/212F8E77-2B24-11D7-8648000102C1865D>.
- [44] Beauchamp Anne-Marie, L'indice Mustang, *Géologie et altération d'une minéralisation aurifère mise en place dans les turbidites de la ceinture de la basse-Eastmain, Eeyou Itschee Baie-James* - ProQuest, Québec, 2018.
- [45] E.W. Sawyer, The influence of source rock type, chemical weathering and sorting on the geochemistry of clastic sediments from the Quetico Metasedimentary Belt, Superior Province, Canada, *Chem. Geol.* 55 (1986) 77–95, [https://doi.org/10.1016/0009-2541\(86\)90129-4](https://doi.org/10.1016/0009-2541(86)90129-4).
- [46] H.W. Nesbitt, G.M. Young, Prediction of some weathering trends of plutonic and volcanic rocks based on thermodynamic and kinetic considerations, *Geochem. Cosmochim. Acta* 48 (1984) 1523–1534, [https://doi.org/10.1016/0016-7037\(84\)90408-3](https://doi.org/10.1016/0016-7037(84)90408-3).
- [47] A. Kishida, R. Kerrich, Hydrothermal alteration zoning and gold concentration at the Kerr-Addison Archean lode gold deposit, Kirkland Lake, Ontario, *Economic Geology* 82 (1987) 649–690, <https://doi.org/10.2113/gsecongeo.82.3.649>.
- [48] X.-C. Li, H.-R. Fan, M. Santosh, F.-F. Hu, K.-F. Yang, T.-G. Lan, Hydrothermal alteration associated with Mesozoic granite-hosted gold mineralization at the Sanshandao deposit, Jiaodong Gold Province, China, *Ore Geol. Rev.* 53 (2013) 403–421, <https://doi.org/10.1016/j.oregeorev.2013.01.020>.
- [49] A. Brochu, *Maîtrise en géologie et génie géologique (1666) en Sciences de la Terre – Profil recherche*, 2021, p. 280.
- [50] R.R. Large, J.B. Gemmill, H. Paulick, D.L. Huston, The alteration box plot: a simple approach to understanding the relationship between alteration mineralogy and lithochemistry associated with volcanic-hosted massive sulfide deposits, *Econ. Geol.* 96 (2001) 957–971, <https://doi.org/10.2113/gsecongeo.96.5.957>.
- [51] W.H. MacLean, T.J. Barrett, Lithochemical techniques using immobile elements, *J. Geochem. Explor.* 48 (1993) 109–133, [https://doi.org/10.1016/0375-6742\(93\)90002-4](https://doi.org/10.1016/0375-6742(93)90002-4).
- [52] P. Mercier-Langevin, Les minéralisations aurifères au sein de la tonalite de La Grande-Sud Baie-James Québec, Université du Québec à Chicoutimi, 2000, <https://doi.org/10.1522/11899414>. Chicoutimi.
- [53] A. Idrus, J. Kolb, F.M. Meyer, Mineralogy, lithochemistry and elemental mass balance of the hydrothermal alteration associated with the gold-rich batu hijau porphyry copper deposit, Sumbawa island, Indonesia, *Resour. Geol.* 59 (2009) 215–230, <https://doi.org/10.1111/j.1751-3928.2009.00092.x>.
- [54] J.-C. Dionne, A. Foucault, J.F. et Raouit, Dictionnaire de géologie, 2, in: Masson (Coll. Guides Géologiques Régionaux), 2<sup>e</sup> édition, Cahiers de géographie du Québec, Paris, 1984, p. 347, <https://doi.org/10.7202/021764ar>, 9 (1985) 460.
- [55] M. Ren, W. Wang, Z. Huang, S. Li, Q. Wu, H. Yu, G. Yuan, P. Sargent, Effect of alteration on the geochemistry and mechanical properties of granite from Pingjiang, Hunan Province, China, *Environ. Earth Sci.* 81 (2022) 1–15, <https://doi.org/10.1007/s12665-022-10197-z>.
- [56] J. Dubé, Caractérisation métallogénique et structurale de la minéralisation aurifère des gisements Triangle et Cheminée No. 4, Val-d'Or, Abitibi, Québec, (n.d.) 259.
- [57] L. Mathieu, Quantifying hydrothermal alteration with normative minerals and other chemical tools at the Beattie Syenite, Abitibi greenstone belt, Canada, *GEEA* 16 (2016) 233–244, <https://doi.org/10.1144/geochem2016-410>.
- [58] B. Rw, *The geochemistry of gold and its deposits*, *Geol. Surv. Can. Bull.* 280 (1979) 584.
- [59] V. Singtuen, B. Phajuy, Geochemistry and alteration of Lampang-Tak volcanic rocks, Thailand (in Suranaree, 29, *J. Sci. Technol.* 29 (5) (2022), 0300811–8.
- [60] A.B. Christie, R.L. Brathwaite, Hydrothermal alteration in metasedimentary rock-hosted orogenic gold deposits, Reefton goldfield, South Island, New Zealand, *Miner. Deposita* 38 (2003) 87–107, <https://doi.org/10.1007/s00126-002-0280-9>.
- [61] P. Mahanta, Remote geochemical alteration proxy for mineral exploration: a case study from Lawa gold mines, India, *J. Asian Earth (Sci.)* 15 (7) (2022), 100093.
- [62] F.P. Bierlein, D.C. Arne, J.M.N. Broome, W.R.H. Ramsay, Metatholeiites and interflow sediments from the Cambrian Heathcote greenstone belt, Australia; sources for gold mineralization in Victoria? *Econ. Geol.* 93 (1998) 84–101, <https://doi.org/10.2113/gsecongeo.93.1.84>.
- [63] M. Arslan, Alteration mineralogy and geochemistry of the hydrothermally altered rocks of the kutlular (sürmene) massive sulfide deposit, NE Turkey, *Turk. J. Earth Sci.* (2009), <https://doi.org/10.3906/yer-0806-7>.
- [64] J. Bogossian, S.G. Hagemann, V.G. Rodrigues, L.M. Lobato, M. Roberts, Hydrothermal alteration and mineralization in the Faina greenstone belt: evidence from the Cascavel and Sertão orogenic gold deposits, *Ore Geol. Rev.* 119 (2020), 103293, <https://doi.org/10.1016/j.oregeorev.2019.103293>.
- [65] V. Singtuen, S. Phajan, A. Anumart, B. Phajuy, K. Srijanta, S. Promkotra, Alteration of high alkaline and alkaline basaltic rocks: parent rocks in the Lava Durian orchard, Sisaket Province, NE Thailand, *Heliyon* 7 (2021).
- [66] N. Gaillard, A.E. Williams-Jones, J.R. Clark, S. Salvi, S. Perrouy, R.L. Linnen, G.R. Olivo, The use of lithochemistry in delineating hydrothermal fluid pathways and vectoring towards gold mineralization in the Malartic district, Québec, *Ore Geol. Rev.* 120 (2020), 103351, <https://doi.org/10.1016/j.oregeorev.2020.103351>.
- [67] L. Djagre, B.G. Koffi, G. Ouattara, Structural analysis of the bagoué furrow (south Boundiali) in the northwest of Ivory Coast: fracturing, Kinematics and Chronology 5 (2022).
- [68] H.A. Helba, K.I. Khalil, N.M.F. Abou, Alteration patterns related to hydrothermal gold mineralization in meta-andesites at dungash area, eastern desert, Egypt, *Resour. Geol.* 51 (2001) 19–30, <https://doi.org/10.1111/j.1751-3928.2001.tb00078.x>.
- [69] D. Xu, T. Deng, G. Chi, Z. Wang, F. Zou, J. Zhang, S. Zou, Gold mineralization in the Jiangnan Orogenic Belt of South China: geological, geochemical and geochronological characteristics, ore deposit-type and geodynamic setting, *Ore Geol. Rev.* 88 (2017) 565–618, <https://doi.org/10.1016/j.oregeorev.2017.02.004>.
- [70] P. Kresten, Granitization - fact or fiction? *Geol. Foren. Stockh. Forh.* 110 (1988) 335–340, <https://doi.org/10.1080/11035898809452668>.
- [71] H. Brisson, Caractéristiques, chronologie et typologie des minéralisations aurifères de la région du Lac Shortt (Québec), sous-province archéenne de l'Abitibi/, Université du Québec à Chicoutimi, Chicoutimi, 1998, <https://doi.org/10.1522/11729184>.
- [72] O. Nadeau, R. Stevenson, M. Jébrak, The archean magmatic-hydrothermal system of lac Shortt (Au-ree), abitibi, Canada: insights from carbonate fingerprinting, *Chem. Geol.* 387 (2014) 144–156, <https://doi.org/10.1016/j.chemgeo.2014.08.021>.
- [73] N. Taghipour, A. Aftabi, R. Mathur, Geology and Re-Os geochronology of mineralization of the miduk porphyry copper deposit, Iran, *Resour. Geol.* 58 (2008) 143–160, <https://doi.org/10.1111/j.1751-3928.2008.00054.x>.
- [74] D.I. Groves, R.J. Goldfarb, M. Gebre-Mariam, S.G. Hagemann, F. Robert, Orogenic gold deposits: a proposed classification in the context of their crustal distribution and relationship to other gold deposit types, *Ore Geol. Rev.* 13 (1998) 7–27, [https://doi.org/10.1016/S0169-1368\(97\)00012-7](https://doi.org/10.1016/S0169-1368(97)00012-7).
- [75] F.M. Meyer, Case histories of orogenic gold deposits, *Minerals* 13 (2023) 369, <https://doi.org/10.3390/min13030369>.
- [76] Z. Liu, X. Mao, H. Deng, B. Li, S. Zhang, J. Lai, R.C. Bayless, M. Pan, L. Li, Q. Shang, Hydrothermal processes at the Axi epithermal Au deposit, western Tianshan: insights from geochemical effects of alteration, mineralization and trace elements in pyrite, *Ore Geol. Rev.* 102 (2018) 368–385, <https://doi.org/10.1016/j.oregeorev.2018.09.009>.
- [77] W. Su, H. Zhang, R. Hu, X. Ge, B. Xia, Y. Chen, C. Zhu, Mineralogy and geochemistry of gold-bearing arsenian pyrite from the Shuiyindong Carlin-type gold deposit, Guizhou, China: implications for gold depositional processes, *Miner. Deposita* 47 (2012) 653–662, <https://doi.org/10.1007/s00126-011-0328-9>.
- [78] W. Zhai, X. Sun, W. Sun, L. Su, X. He, Y. Wu, Geology, geochemistry, and genesis of Axi: a Paleozoic low-sulfidation type epithermal gold deposit in Xinjiang, China, *Ore Geol. Rev.* 36 (2009) 265–281, <https://doi.org/10.1016/j.oregeorev.2009.04.003>.